Visual Instruction Bottleneck Tuning

Changdae Oh [1] **Jiatong Li** [1] **Shawn Im** [1] **Yixuan Li** [1]

Abstract

Despite widespread adoption, multimodal large language models (MLLMs) suffer performance degradation when encountering unfamiliar queries under distribution shifts. Existing methods to improve MLLM generalization typically require either more instruction data or larger advanced model architectures, both of which incur non-trivial human labor or computational costs. In this work, we take an alternative approach to enhance the robustness of MLLMs under distribution shifts, from a representation learning perspective. Inspired by *information bottleneck (IB) principle*, we derive a variational lower bound of the IB for MLLMs and devise a practical implementation, ***Visual Instruction Bottleneck Tuning*** (`Vittle`). We then provide a theoretical justification of `Vittle` by revealing its connection to an information-theoretic robustness metric of MLLM. Empirical validation of three MLLMs on open-ended and closed-form question answering and object hallucination detection tasks over 45 datasets, including 30 shift scenarios, demonstrates that `Vittle` consistently improves the MLLM's robustness under shifts by pursuing the learning of a minimal sufficient representation.

1. Introduction

In intensive races on the track of frontier-level AI models, we have observed unprecedented achievements through the form of a general-purpose chat assistant known as multimodal large language models (MLLMs) (xAI, 2025; OpenAI, 2025; Google Cloud, 2025) that combine a visual encoder with a large language model. Their universal yet flexible question-answering interface enables MLLMs to easily permeate our lives from general problem-solving (Liang et al., 2024; Yang et al., 2024b) to practical applications (Al-Saad et al., 2024; Li et al., 2024d; Caffagni et al., 2024; Cui et al., 2024a). While these models may achieve human-like or even surpass human-level performance on certain tasks, a critical gap remains in their robustness—particularly in handling input variations that humans process effortlessly.

Human intelligence thrives on the ability to distill a large amount of sensory and cognitive inputs into concise abstract representations, a process akin to *conceptual compression* (Turner, 2006; Gray & Tall, 2007). By prioritizing sparse salient features while discarding redundancy, humans can shape a robust prototypical representation of complex data instances that captures a proper level of **invariance to low-level superficial features** for generalization, yet maintains **sensitivity to high-level abstract features** for discrimination (Miller, 1956; Rosch, 1975; Zhaoping, 2025). Unfortunately, there are consistent reports implying that the current MLLMs still lag far behind this desired trade-off between invariance and sensitivity (Zhang et al., 2024; Han et al., 2024b; Ye-Bin et al., 2025; Oh et al., 2025a).

Specifically, MLLMs fail to produce relevant responses under query distribution shifts. That is, they are vulnerable to processing subtly perturbed samples and long-tail samples (Oh et al., 2025a). This limitation partially stems from the difficulty of acquiring diverse high-quality multimodal instruction data at scale. When trained via standard maximum likelihood estimation on this relatively limited amount of instruction data, MLLM tends to fit to data-specific patterns and result in a brittle solution (Geirhos et al., 2020; Ye et al., 2024; Liang et al., 2025). To enhance generalization, existing efforts typically fall into two categories (1) *data-centric* approaches, which collect more instruction data (Zhao et al., 2023; Li et al., 2024b; Gu et al., 2024) and processes input in a finer granularity (Liu et al., 2024c; Shen et al., 2025), and (2) *model-centric* approaches, which scale up the underlying model using more expressive or specialized backbones (Chen et al., 2024b; Tong et al., 2024a; Shi et al., 2025; Bai et al., 2025b). However, both data scaling and model scaling are resource-intensive—requiring significant annotation or computational cost.

In this work, we propose a new approach from a *representation-centric* view to improve the robustness of MLLMs under distribution shifts. Rather than scaling

[*]Equal contribution [1]Department of Computer Sciences, University of Wisconsin–Madison, WI, USA. Correspondence to: Changdae Oh <changdae@cs.wisc.edu>, Yixuan Li <sharonli@cs.wisc.edu>.

Published at ICML 2025 Workshop on Reliable and Responsible Foundation Models. Copyright 2025 by the author(s).

data or model, we introduce a lightweight, theoretically grounded module that enhances the internal representations of MLLMs via the information bottleneck (IB) principle. While the IB framework has been explored in small-scale or classification settings (Alemi et al., 2017; Vera et al., 2018; Wu et al., 2020; Mahabadi et al., 2021; Li et al., 2025), integrating it to autoregressive multimodal instruction tuning poses unique challenges due to the complexity of modeling mutual information across high-dimensional, sequential, and heterogeneous modalities. We overcome these barriers by formulating a novel variational lower bound of the IB objective specifically tailored to the multimodal and sequential nature of MLLMs. We further instantiate this formulation as a modular and scalable implementation—***Visual Instruction Bottleneck Tuning*** (`Vittle`), which inserts a simple bottleneck layer within the LLM backbone. `Vittle` pursues *minimal sufficient representations* (Cover, 1999) that try to preserve response-relevant information only while discarding nonessential residual features. To our knowledge, this is the first work to investigate the IB framework for end-to-end instruction tuning of multimodal LLMs, offering a model-agnostic pathway toward building robust AI systems.

We conduct an extensive evaluation of `Vittle` across a wide spectrum of multimodal benchmarks to assess its robustness and generalization under distribution shift. Our experiments span 30 distribution shifts covering diverse forms of perturbation (in both vision and language) and long-tail distributions. Through these evaluations, we demonstrate that `Vittle` consistently improves robustness over standard instruction tuning baselines, without sacrificing performance on standard benchmarks and canonical tasks. Notably, we find that the bottlenecked representations induced by `Vittle` lead to enhanced invariance in the latent space, aligning semantically similar inputs more closely—even under input shifts—while reducing overfitting to modality-specific artifacts. We also show that `Vittle` is compatible with different MLLMs, offering robustness gains while maintaining similar inference-time cost. These results underscore the practical benefit and theoretical promise of information-regularized representation learning for robust multimodal instruction tuning.

Contributions: (1) We propose a new representation-centric framework for improving the robustness of MLLMs under distribution shifts, grounded in the information bottleneck principle. (2) We explore the IB-based end-to-end learning objective of an MLLM for the first time by inducing a new variational lower bound of IB for MLLM and devising a practical instantiation, `Vittle`, supported by theoretical analysis. (3) Through experiments on 30 diverse types of distribution shifts, we thoroughly validate the robustness of MLLMs on open-ended/closed-form QA and object hallucination detection tasks and show advantages of compressive representation induced by pursuing the IB principle.

2. Background, Related Work, and Motivation

Multimodal large language models (MLLMs). Recent advances in MLLMs integrate a pre-trained language model with a vision encoder through *visual instruction tuning* (Liu et al., 2023; Dai et al., 2023). To be specific, let $X = (X_v, X_t)$ denote a multimodal input query consisting of visual and textual input, e.g., an image and a corresponding instruction or a question given that image, and Y denote a desired response given the input query. An MLLM f_θ with parameter θ is trained to produce the desired response given an input query with a conditional autoregressive language modeling objective, i.e., $\arg\min_\theta \mathbb{E}_{X,Y}[\sum_{m=1}^{M} \log f_\theta(Y_m|X_v, X_t, Y_{<m})]$ for a sequence of M-length responses, where the visual input X_v go through a visual encoder and projector modules to be converted as a sequence of tokens that have the same dimension as text embeddings and can be processed by an LLM backbone[1]. After being trained, these models process a wide array of multimodal instructions to solve arbitrary visual question answering tasks (Lee et al., 2024).

Robustness problem in MLLMs. Despite their impressive performance on standard benchmarks and their growing deployment in real-world applications (Li et al., 2024d;c; Raza et al., 2025), MLLMs remain vulnerable to input perturbations (Qiu et al., 2024; Cui et al., 2024b; Verma et al., 2024). For example, MLLMs undergo a systematic performance drop (Oh et al., 2025a) when they encounter samples of superficial perturbations (e.g., varying brightness of image and typo in text) illustrated in Figure 1 (a). As shown in the bar plot of Figure 1 (b), LLaVA-v1.5-7B model undergoes severe performance degradation on LLaVA-Bench-COCO (LB-COCO; Liu et al. (2023)) under the perturbations from visual input, textual input, and their joint (V, T, and J Pert), which poses severe threats given current broad AI application ecosystems.

We posit that these vulnerabilities arise from the way MLLMs structure their internal representation space. In particular, inputs affected by perturbations are often embedded far from their intact (clean) counterparts, reflecting a distribution shift in the representation space that leads to poor generalization from an information-theoretic perspective (Oh et al., 2025a). The right side of Figure 1 (b) illustrates this phenomenon: using LLaVA-v1.5, we visualize representations of LB-COCO alongside its challenging variant, where the image and text inputs are perturbed. In this setting, semantically equivalent examples are mapped to distinct and distant regions in the latent space, *suggesting a lack of invariance to superficial input variations, which is crucial for robustness to distribution shifts*.

[1]For simplicity, we will omit the visual encoder and projector in our learning objective at following sections.

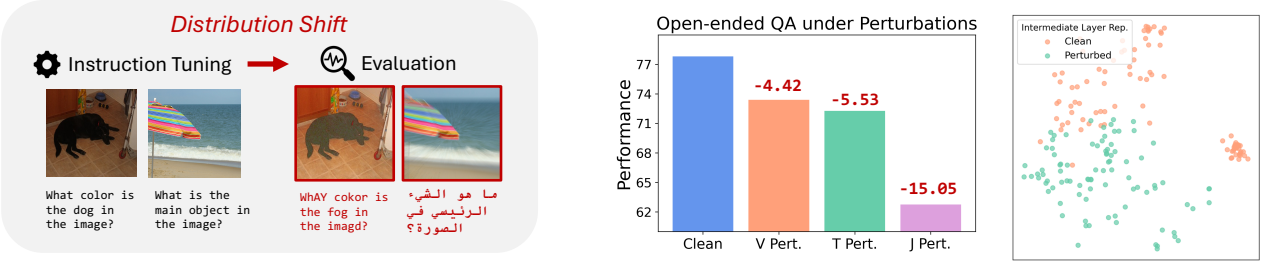

(a) MLLM encounters distribution shifts (b) Distribution shifts result in MLLM performance drops

Figure 1: **Illustration of distribution shifts for an MLLM (a) and performance degeneration and embedding shifts of the MLLM (b).** An MLLM (LLaVA-v1.5-7B) receives arbitrary queries that might be visually and/or textually perturbed by unexpected noise. These distribution shifts result in performance drops, as shown in the middle bar plot. A visualization of intermediate layer representations of the MLLM on LLaVA-Bench-COCO and its variants indicates that MLLM fails to learn a proper level of invariance to generalize multimodal queries in the representation space.

Motivated by this, our work aims to enhance the robustness of MLLMs by explicitly regularizing their internal representations, encouraging them to retain task-relevant information while discarding input-specific noise—thereby finding a good balance between invariance to low-level superficial features and sensitivity to high-level abstract features for better generalization.

Information bottleneck principle. The information bottleneck framework provides a principled approach to measure the quality of representations that are maximally predictive of a target variable while compressing redundant information from an input variable (Tishby et al., 2000; Tishby & Zaslavsky, 2015). Numerous works have explored the use of IB training objective (Alemi et al., 2017), across computer vision (Luo et al., 2019; Federici et al., 2020), natural language processing (Mahabadi et al., 2021; Li et al., 2025), graph learning (Wu et al., 2020; Miao et al., 2022), and time-series modeling (Liu et al., 2024d). These efforts are supported by theoretical insights suggesting that optimizing for the IB objective can reduce generalization error (Vera et al., 2018; Kawaguchi et al., 2023). However, most prior work focused on classification settings (Mahabadi et al., 2021; Li et al., 2025) and/or relatively small-scale models (Alemi et al., 2017; Wang et al., 2021; Mahabadi et al., 2021). Although a recent study explored IB for MLLMs (Bai et al., 2025a), the authors adopted IB training on a lightweight projector module while keeping the LLM backbone frozen. In contrast, *our work is the first to investigate the IB framework for end-to-end training of large-scale autoregressive multimodal language models*. Beyond shallow adaptations, we directly modify the internal structure of the LLM to promote IB-consistent behavior throughout the training process. We focus specifically on instruction tuning for MLLMs—which have become increasingly central to modern AI ecosystems but remain largely unexplored from the perspective of IB-based learning.

3. Method

3.1. Preliminary: Information Bottleneck As a Learning Objective

Let X be a multimodal input query (e.g., image-text pair), Y the desired output, and $Z = f(X)$ an intermediate representation extracted by the MLLM encoder $f(\cdot)$. The Information Bottleneck principle aims to learn representations that are *maximally informative about the output* Y while being *minimally informative about the input* X. Formally, this is expressed as the optimization objective:

$$\max_f \mathrm{IB}_f(X, Y) = I(Z, Y) - \beta I(Z, X) \tag{1}$$

where $I(\cdot, \cdot)$ denotes mutual information and β is the trade-off coefficient. Minimizing $I(Z, X)$ encourages removing redundant or input-specific variations, while maximizing $I(Z, Y)$ ensures that the representation retains task-relevant signals necessary to predict the desired output.

In other words, the IB objective promotes representations that discard non-essential features tied to the input modality, while preserving those critical for solving the task. This property is particularly desirable for robust instruction tuning, where diverse multimodal inputs must be mapped to consistent, meaningful outputs under varied conditions (e.g., visual and textual perturbations). Despite its appeal, integrating the IB objective into MLLM training is ***highly non-trivial due to the intractability of mutual information estimation and the complexity of autoregressive and multimodal architectures***.

3.2. Variational Inference for Information Bottleneck in MLLMs

Directly optimizing the IB objective is generally intractable, as it involves mutual information terms over unknown data distributions. In this work, we introduce a tractable variational bound on the IB objective, specifically tailored to the

autoregressive and multimodal structure of MLLMs. We outline the key steps below and provide full derivations in the Appendix C.

We begin with the mutual information term $I(Z, X)$. Given the sequential nature of MLLMs, we decompose both the input $X = (X_v, X_t)$ and the latent representation $Z = (Z_v, Z_t)$ into **v**isual and **t**extual components. We can then derive the following upper bound for $I(Z, X)$:

$$\begin{aligned} I(Z,X) &= \mathbb{E}_{x,z}[\log \frac{p(z|x)}{p(z)}] \leq \mathbb{E}_{x,z}[\log \frac{p(z|x)}{r(z)}] \\ &= \mathbb{E}_{x_v,x_t,z_v,z_t}[\log \frac{p(z_t|x_v,x_t)p(z_v|x_v)}{r(z_v)r(z_t)}] \\ &= \mathbb{E}_{x_v,x_t}[\mathbb{E}_{z_t|x_v,x_t}[\mathbb{E}_{z_v|x_v}[\log \frac{p(z_v|x_v)}{r(z_v)}]]] \\ &+ \mathbb{E}_{x_v,x_t}[\mathbb{E}_{z_v|x_v}[\mathbb{E}_{z_t|x_v,x_t}[\log \frac{p(z_t|x_v,x_t)}{r(z_t)}]]] \\ &= \mathbb{E}_{x_v}[D_{\mathrm{KL}}(p(z_v|x_v)||r(z_v))] \\ &+ \mathbb{E}_{x_v,x_t}[D_{\mathrm{KL}}(p(z_t|x_v,x_t)||r(z_t))], \end{aligned} \tag{2}$$

where the first inequality holds given the non-negativity of Kullback-Leibler divergence (KLD), $D_{\mathrm{KL}}(r(z)||p(z))$, and $p(z_v|x_v, x_t) = p(z_v|x_v)$ due to causal attention in MLLM. We introduce $r(z) = r(z_v, z_t) = r(z_v)r(z_t)$ as a factorizable variational approximation of the true prior $p(z)$.

Next, for the output-relevant term $I(Z, Y)$, we have the lower bound:

$$\begin{aligned} I(Z,Y) &= \mathbb{E}_{y,z}\left[\log \frac{p(y|z)}{p(y)}\right] \\ &\geq \mathbb{E}_{x,y,z}\left[\log q(y|z)\right] - \mathbb{E}_{y}[\log p(y)] \\ &\geq \mathbb{E}_{x,y}\left[\mathbb{E}_{z|x}\left[\log q(y|z)\right]\right], \end{aligned} \tag{3}$$

where we replace the true posterior $p(y|z)$ with a variational approximation $q(y|z)$ that will be parameterized by a model (will be elucidated in Section 3.3).

Finally, combining the lower bound of $I(Z, Y)$ and the upper bound of $I(Z, X)$ yields a variational lower bound for the IB objective as follows,

$$\begin{aligned} \mathrm{IB}(X,Y) \geq\ & \mathbb{E}_{x,y}\left[\mathbb{E}_{z|x}[\log q(y|z)]\right] \\ & - \beta\left(\mathbb{E}_{x_v}\left[D_{\mathrm{KL}}(p(z_v|x_v)||r(z_v))\right]\right. \\ & \left. + \mathbb{E}_{x_v,x_t}\left[D_{\mathrm{KL}}(p(z_t|x_v,x_t)||r(z_t))\right]\right), \end{aligned} \tag{4}$$

In the next section, we elaborate on how we can implement this variational lower bound for MLLM instruction tuning in practice.

3.3. `Vittle`: A Practical Implementation of Visual Instruction Bottleneck Tuning

By using Monte Carlo approximation of expectations over data, Eq. (4) can be expressed as follows,

$$\begin{aligned} \mathcal{L}_\beta = & \frac{1}{N}\sum_{i=1}^{N}\mathbb{E}_{z|x^i}[\log q(y^i|z)] \\ & - \beta\left(D_{\mathrm{KL}}(p(z_v|x_v^i)||r(z_v)) + D_{\mathrm{KL}}(p(z_t|x_v^i,x_t^i)||r(z_t))\right). \end{aligned} \tag{5}$$

To compute this empirical estimate of the IB lower bound, we need to model the posterior distributions, $p(z_v|x_v)$ and $p(z_t|x_v, x_t)$, and prior distributions $r(z_v)$ and $r(z_t)$, of the MLLM's inner representation Z. While in principle these distributions can take arbitrary forms, multivariate Gaussian distributions have been widely adopted in variational inference and probabilistic embedding literature (Graves, 2011; Kingma & Welling, 2014; Blei et al., 2017; Alemi et al., 2017; Oh et al., 2019; Chun et al., 2021) due to their mathematical tractability and empirical effectiveness. By following this common standard, we set the posteriors and priors as Gaussian with diagonal covariance for d-dimensional variable, and will elucidate how exactly they are defined below.

Posterior distributions. As illustrated in Figure 2, we parameterize the posteriors $p(z_v|x_v)$ and $p(z_t|x_v, x_t)$ using simple MLP blocks. Specifically, we introduce two nonlinear projections, $g_{\phi_v}, g_{\phi_t} : \mathbb{R}^d \to \mathbb{R}^{2d}$, which map each d-dimensional token embedding to the posterior Gaussian parameter vectors $\mu \in \mathbb{R}^d$ and $\sigma^2 \in \mathbb{R}^d_+$ for the vision and language modalities, respectively. Given an intermediate l-th layer representation $(z_v, z_t) = f_{\theta^l}(x_v, x_t)$, we define:

$$p(z_v|x_v) = \mathcal{N}(z_v; \mu_v, \sigma_v^2 \cdot I), \quad p(z_t|x_v, x_t) = \mathcal{N}(z_t; \mu_t, \sigma_t^2 \cdot I),$$

where $[\mu_v, \sigma_v^2] = g_{\phi_v}(f_{\theta^l}(x_v))$ and $[\mu_t, \sigma_t^2] = g_{\phi_t}(f_{\theta^l}(x_v, x_t))$, with the mean and variance parameters split along output dimensions of MLP. These MLPs are applied position-wise in the same manner as Transformer's feed-forward layers (Vaswani et al., 2017), producing token-wise variational posteriors. Now, we can sample from the posterior distributions of MLLM representation by $\tilde{z}_v \sim p(z_v|x_v)$ and $\tilde{z}_t \sim p(z_t|x_v, x_t)$. Then, to strike a balance between invariance and sensitivity, we interpolate the original representation z (pre-bottleneck) with its bottlenecked counterpart $\tilde{z}$ as $\hat{z} = (1 - \alpha)z + \alpha\tilde{z}$. These representations are fed into the remaining layers to compute the predictive distribution over outputs, i.e., $q(y|z) := f_{\theta^{l+}}(y|\hat{z}_v, \hat{z}_t)$. While direct sampling introduces non-differentiability, we can enable the gradient flow using the reparameterization trick (Kingma & Welling, 2014) to sample $\tilde{z}$ via $\tilde{z} = \mu + \sigma \odot \epsilon$ with $\epsilon \sim \mathcal{N}(\mathbf{0}, I)$ where μ and σ are the outputs of the bottleneck MLP module given input x.

Prior distributions. We consider two instantiations of the prior distribution for both Z_v and Z_t: (1) a *fixed* standard Gaussian $\mathcal{N}(\mathbf{0}, I)$, which is input-independent and enforces strong isotropy, and (2) a *learnable* Gaussian $\mathcal{N}(\mu_\psi, \sigma_\psi^2 \cdot I)$, where μ_ψ and σ_ψ^2 are two learnable vectors shared across samples. Each prior affects the formation of representations differently—the fixed prior imposes stronger regularization and robustness, while the learnable prior introduces additional flexibility by allowing the model to adapt to the instruction tuning distribution. We name the former `Vittle`

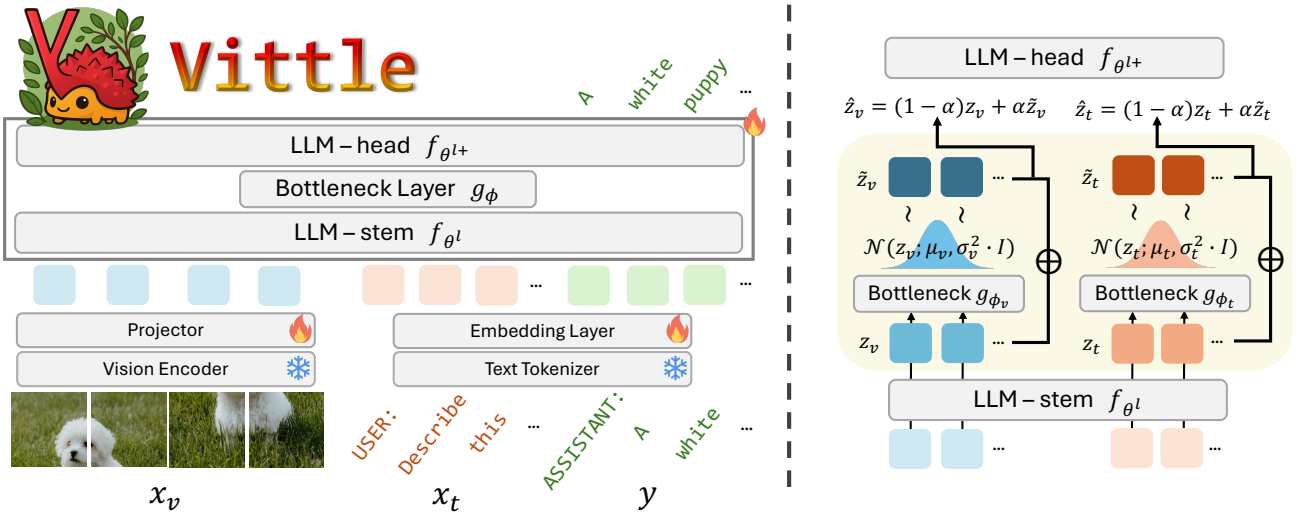

Figure 2: **`Vittle` architecture**. We insert a learnable bottleneck layer $g_\phi = \{g_{\phi_v}, g_{\phi_t}\}$ on top of l blocks of LLM backbone (i.e., LLM-stem f_{θ^l}) to estimate posterior distributions of token embeddings. After obtaining a sample per token $\{\tilde{z}_v, \tilde{z}_t\}$ from posteriors, we interpolate it with a pre-bottlenecked token representation $\{z_v, z_t\}$ and pass it through the remaining LLM blocks (i.e., LLM-head $f_{\theta^{l+}}$).

(F) and the latter `Vittle` (L), and validate them altogether for all the evaluations in Section 4.

Overall objective and implementation. The first term of $\mathcal{L}_\beta$(Eq. (5)) can be easily computed through the standard cross-entropy, and our Gaussian instantiation of posterior and priors allows us to derive closed-form expressions of KLD terms that can be computed from simple arithmetic between μ and σ^2 parameters (See Appendix A.2). We set $\beta = \frac{0.1}{d}$ where d is the hidden dimension of the MLLM, to normalize the KL regularization terms relative to the size of the latent dimension. The interpolation coefficient α in $\hat{z} = (1-\alpha)z + \alpha\tilde{z}$ increases progressively following a cosine schedule up to 0.5. During inference, we consistently use an averaged representation $\hat{z} = (z + \tilde{z})/2$. The target layer to apply the bottleneck module can differ between visual and textual tokens, but we set $l = 24$ for both modalities among 32 layers in a 7B-size LLM, i.e., top 25% layer, by default for simplicity (See Appendix B.1 for the ablation study). Figure 2 depicts the architecture overview.

3.4. Theoretical Justification

The learning objective of `Vittle` has an attractive theoretical interpretation that can support the improvement in robustness of `Vittle`. In this section, we first introduce a recently proposed information-theoretic measure of MLLM's robustness under distribution shifts, ***effective mutual information difference*** (EMID (Oh et al., 2025a)), and show how `Vittle` can contribute to improving EMID.

Definition 3.1 (EMID). Let $P_\Theta : \mathcal{X} \to \mathcal{Y}$ be an MLLM with parameters Θ that produces an output response Y_Θ given an input instruction X. For joint distributions P_{XY} and Q_{XY}, effective mutual information difference of P_Θ over P and Q is defined as below,

$$\begin{aligned}&\text{EMID}(P_{XY}, Q_{XY}; P_\Theta)\\ &:= [I(P_{XY_\Theta}) - I(P_{XY})] - [I(Q_{XY_\Theta}) - I(Q_{XY})]. \quad (6)\end{aligned}$$

where $I(\cdot)$ denotes mutual information that measures the relevance between input instruction and response. A higher value of EMID indicates that MLLM P_Θ undergoes performance degeneration in the distribution Q (test data) compared to P (training data), so we want to achieve a lower value of it to ensure robustness. We now derive an upper bound for EMID (See Appendix D for the proof).

Proposition 3.2 (EMID upper bound). *Let P_Θ be an MLLM that maps $X = \{X_v, X_t\}$ to $Z = \{Z_v, Z_t\}$, and then sequentially maps Z to Y_Θ. Given joint distributions $P_{XY} = P_X \times P_{Y|X}$ and $Q_{XY} = Q_X \times Q_{Y|X}$ (resp. P_{ZY} and Q_{ZY}), by assuming consistent conditionals over $Z_v|Z_t$, $Z_t|Z_v$, and $Y|X$ between P and Q, we have an upper bound for EMID$(P_{XY}, Q_{XY}; P_\Theta)$ as below,*

$$\begin{aligned}&\hat{H}\left(D_{\text{JS}}^{\frac{1}{2}}(P_{Z_v}||Q_{Z_v}) + D_{\text{JS}}^{\frac{1}{2}}(P_{Z_t}||Q_{Z_t}) + \sqrt{\Delta_{X|Z}}\right)\\ &+ |H(P_{Y_\Theta}) - H(P_Y)| + |H(Q_{Y_\Theta}) - H(Q_Y)|, \quad (7)\end{aligned}$$

where H and $D_{\text{JS}}^{\frac{1}{2}}$ indicate the entropy and square root of Jensen-Shannon divergence (JSD), respectively, $\Delta_{X|Z} := \mathbb{E}_{z\sim P}[D_{\text{KL}}(P_{X|z}||M_{X|z})] + \mathbb{E}_{z\sim Q}[D_{\text{KL}}(Q_{X|z}||M_{X|z})]$ with a mixture distribution $M = \frac{P+Q}{2}$, and $\hat{H} := \max_{x\in\mathcal{X}}[H(Q_{Y|x}) + H(P_{Y_\Theta})]$. As we consider an optimization problem of Θ, the terms, $H(P_Y)$, $H(Q_Y)$, and $\max H(Q_{Y|X})$, can be ignored from Eq. 7. We can also ignore $\sqrt{\Delta_{X|Z}}$ term because it cannot directly affect Y_Θ given the Markov assumption $X \to Z \to Y_\Theta$.

Implication. `Vittle` maximizes the variational lower bound of IB, which consists of (1) minimizing a standard negative log-likelihood term representing an expected risk, and (2) minimizing KLD terms to enforce posterior distributions close to prior distributions. By pursuing (1), MLLM P_Θ seeks a solution Θ that minimizes the expected risk and reduces its output entropy $H(P_{Y_\Theta})$ and $H(Q_{Y_\Theta})$ (Wen et al., 2024; Yang et al., 2024a; Groot & Valdenegro-Toro, 2024). Besides, it also reduces JSD between representation distributions P_Z and Q_Z by promoting all posterior samples to be laid near the pre-defined priors. In summary, reduced entropy and JSD terms induce lower EMID, which means that `Vittle` tries to achieve minimal difference between effective mutual information over training and evaluation distributions, while adapting to the in-distribution training set.

We show that `Vittle` indeed reduces JSD and EMID under distribution shifts in Table 4, and demonstrate in Section 4.2 that `Vittle`'s nice theoretical property is translated into consistent robustness gains under 30 distribution shift scenarios while maintaining in-distribution task performance.

4. Experiment

4.1. Setup

Model and implementation detail. We adopt LLaVA-v1.5 (Liu et al., 2024b) as our main baseline MLLM, where we set CLIP ViT-L/14-336px (Radford et al., 2021) as a vision encoder, Vicuna-v1.5-7B (Chiang et al., 2023) as an LLM, and a two-layer MLP as a projector. We follow the standard two-stage training of LLaVA (Liu et al., 2023), and replicate stage-1 for image-text alignment with the same configuration and dataset (`LLaVA-pretrain-558k`) of LLaVA-v1.5 (Liu et al., 2024b). Then, on the `LLaVA-mix-665k`, we apply our `Vittle` objective. To validate the scalability and broad applicability, we also consider LLaVA-v1.5-13B and Prism-7B (Karamcheti et al., 2024). Refer to Appendix A for details and Appendix B for LLaVA-v1.5-13B and Prism-7B results, respectively.

Task, metric, and datasets. We evaluate instruction-tuned MLLMs with three representative tasks: (1) *open-ended question answering*, (2) *object hallucination detection*, and (3) *closed-form question answering*. All are formatted as a question answering (QA) with a single image input, where we use the average relative preference score measured by GPT-4o LLM judge (Zheng et al., 2023) with three repeated runs for open-ended QA, while using exact matching accuracy for hallucination detection and closed-form QA. For open-ended QA tasks, we adopt four datasets: LB-COCO (Liu et al., 2023) as a *clean and typical* dataset, and LLaVA-Bench in-the-wild (LB-Wild), LLaVA-Bench-Wilder (LB-Wilder), and WildVision-Bench (WV-Bench) as *long-tail* datasets. Then, we apply 27 types of image and text perturbations on LB-COCO samples[2] to yield 28 variants of *perturbed* LB-COCO (one of clean and nine of visual, textual, and joint perturbations, respectively). For object hallucination detection tasks, we adopt POPE (Li et al., 2023) as a *clean and typical* dataset. Then, we generate nine variants of *perturbed* POPE with visual perturbations. Here, we consider the LB-COCO and POPE as in-distribution (ID) datasets because they are generated from MS-COCO samples that construct majorities of the instruction tuning set of modern MLLMs, including LLaVA. For closed-form QA, we adopt four representative datasets: ScienceQA (Lu et al., 2022), MMMU (Yue et al., 2024), MME (Liang et al., 2024), and MMStar (Chen et al., 2024a). In summary, we experiment with **45 datasets** (31 of open-ended, 10 of object hallucination detection, and 4 of closed-form tasks).

4.2. Results

Vittle improves robustness under input perturbations. We first evaluate `Vittle` on object hallucination detection tasks with nine variants of POPE perturbed by visual corruptions in Figure 3. Although MLLMs trained with a standard objective and `Vittle` similarly suffer from perturbations, two instantiations of `Vittle` consistently outperform the standard objective. Interestingly, `Vittle` outperforms the baseline even in clean POPE (See Appendix B). We speculate that `Vittle`'s information control prevents the reliance on a partial feature of a single modality (Rahmanzadehgervi et al., 2024), e.g., textual feature, which is a common source of hallucination.

Next, we present the validation on the open-ended QA task with 18 types of input perturbations, which are applied to visual and textual input independently or simultaneously in Figure 4. As we can see, `Vittle` greatly enhances performance in various perturbation datasets highlighted by green numbers that indicate the relative improvements of `Vittle` (F) compared to the baseline. Among the two variants of `Vittle`, `Vittle` (F) showcases better generalization under perturbations than `Vittle` (L), suggesting the benefits of a conservative zero-centered isotropic prior distribution to address a variety of subtle input perturbations. Next, we further explore `Vittle`'s robustness by evaluating varying perturbation severity. To be specific, we generate perturbations on three different degrees that determine how significantly the image or text would be changed. In Figure 5, we see that `Vittle` achieves better performance in general, where the margin becomes larger under severe perturbations. In summary, we observe a consistent

[2] See Appendix A.3 for a comprehensive summary of all perturbations and their generation processes.

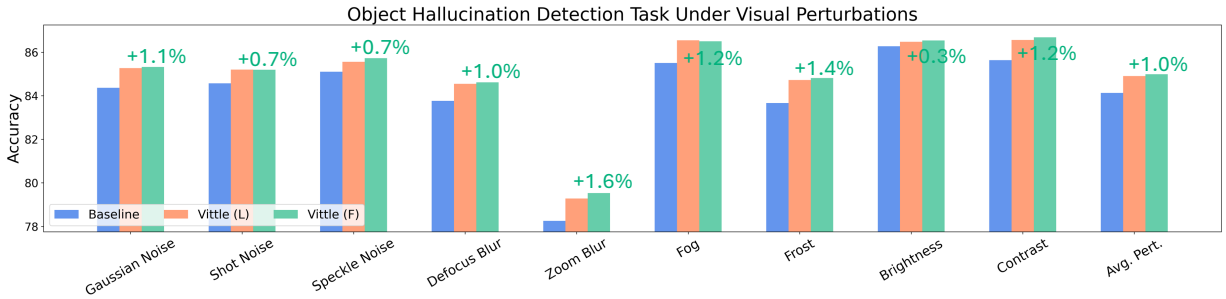

Figure 3: **Object hallucination detection performance on POPE variants**. We enumerate the hallucination detection accuracy of each method on nine versions of perturbed samples, and observe consistent gains by `Vittle` (highlighted by green numbers of relative improvement from baseline).

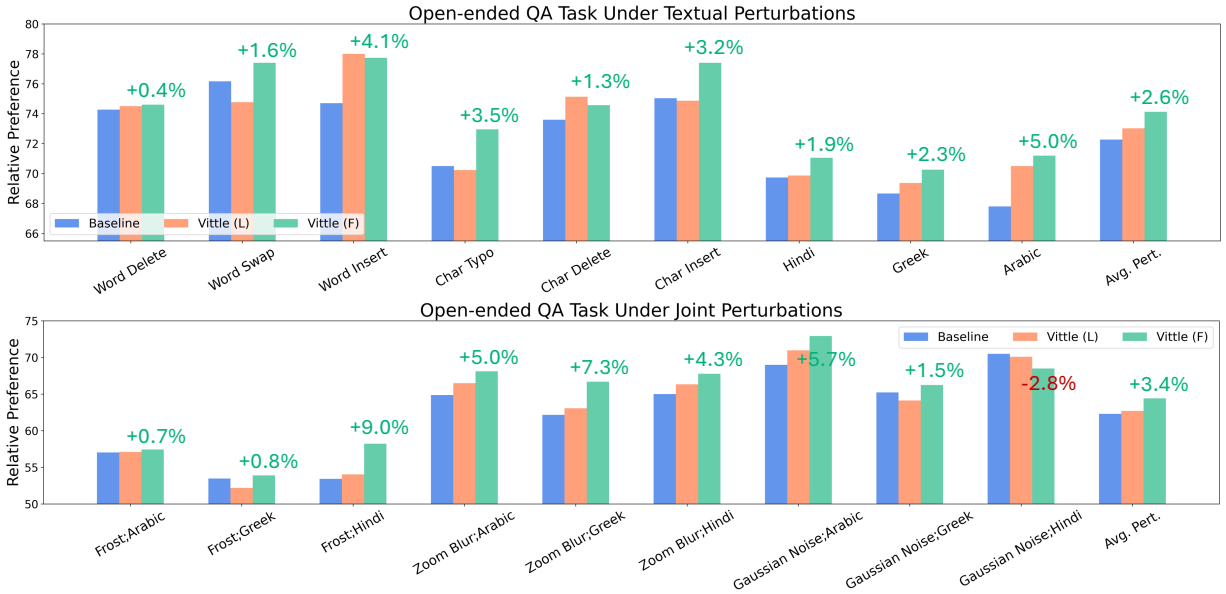

Figure 4: **Open-ended QA performance on LB-COCO variants**. We enumerate the relative preference score of responses from each model on 18 version of perturbed samples, and observe consistent gains by `Vittle` (especially for the `Vittle` (F)) on most of the textual (top), and joint (bottom) perturbations (results on visual perturbations are in Appendix B).

gain by `Vittle` on the perturbed input setting across two tasks, which indicates that `Vittle` enhances the robustness to distribution shifts by pursuing the minimality of data representation.

Vittle improves generalization to long-tail distributions. Not only subtle perturbations on input, but long-tail samples are also commonly encountered in many MLLM applications. In Table 1, we validate `Vittle` on three long-tail QA tasks constructed with real-world user queries. We see that `Vittle` also excels in generalizing long-tailed samples compared to the baseline. Interestingly, `Vittle` (L)–learnable prior–exhibits better performance compared with `Vittle` (F). We speculate that a learnable prior IB guides the model to learn a better sensitivity for high-level abstractions as well as an invariance to low-level noise by allowing additional flexibility to shape data-driven priors, yielding superior performance on tasks that require in-depth understanding of irregular queries.

Table 1: **Performance comparison on long-tail open-ended QA tasks** those contain queries that are quite different from typical training samples in terms of visual content and textual semantics.

Method	LB-Wild	LB-Wilder	WV-Bench
Baseline	51.6	156.9	60.0
`Vittle` (L)	**54.6**	**168.8**	**60.4**
`Vittle` (F)	52.2	166.1	59.7

Vittle preserves competitive performance on general benchmarks. Although the main focus of `Vittle` is to improve the model's robustness under distribution shifts, securing the rich multimodal understanding capability and knowledge to diverse disciplines is also crucial as an essence of MLLM. To validate the multimodal understanding with an advanced level of knowledge, we evaluate each method on four representative closed-form QA benchmark datasets

Table 2: **Performance comparison on general benchmark datasets**. These four multi-choice QA datasets require a higher level of multimodal understanding across multiple domains.

Method	SciQA	MMMU	MME	MMStar	Avg.
Baseline	64.6	**35.6**	69.7	**33.7**	50.9
Vittle (L)	64.7	35.3	**70.5**	**33.7**	**51.1**
Vittle (F)	**65.4**	34.5	70.1	33.5	50.9

Table 3: **Comparison with weight-space compression methods.** We compare Vittle with the LoRA and weight decay (WD) methods on LB-COCO and its perturbed variants.

Method	Clean	V Pert.	T Pert.	J Pert.
Baseline	77.8	73.4	72.2	62.3
LoRA	73.4	70.4	62.7	39.7
WD	74.1	72.1	73.0	59.5
Vittle (L)	76.7	73.9	73.0	62.7
Vittle (F)	76.1	**74.2**	**74.1**	**64.4**

covering various fields. In Table 2, we observe that Vittle shows competitive performance with the standard approach, which implies that Vittle can also be used as a general-purpose learning objective.

Comparison with alternative learning approaches. Note that the regularization forced by Vittle works on the representation space to penalize the amount of information encoded in the data representations. One of the natural alternatives is to regularize the model weight directly. In Table 3, we compare Vittle with LoRA (Hu et al., 2022) and the weight decay method (WD) as instantiations of weight-space regularization, and the results suggest that explicit regularization on weight-space does not ensure a good

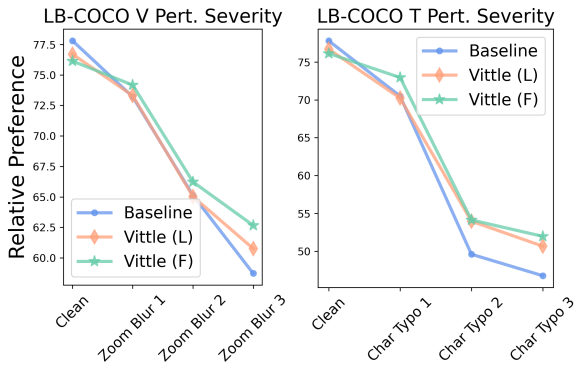

Figure 5: **Evaluation under varying perturbation severity.** Vittle achieves better performance, especially on severe perturbations.

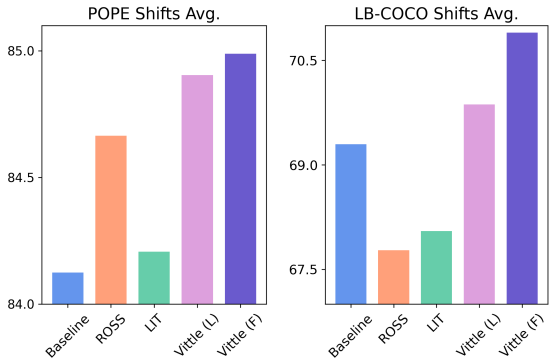

Figure 6: **Comparison with other objective functions.** We report the average performance for all perturbations in POPE and LB-COCO.

balance between adaptability on in-distribution and robustness to distribution shifts. The other line of alternatives is ***information maximization*** during visual instruction tuning (Wang et al., 2025; Zhou et al., 2025), which is the exact opposite of Vittle's design principle. We compare two recent methods of this, ROSS (Wang et al., 2025) and LIT (Zhou et al., 2025), with Vittle on LB-COCO and POPE under perturbations. As shown in Figure 6, although these approaches are effective in improving object hallucination detection performances, they fail to achieve competitive performance on the open-ended QA task (See Appendix B for more results). This implies the non-trivial challenge of devising a general learning objective for MLLMs that can consistently improve robustness across diverse tasks, where we can see the promise of Vittle towards broadly applicable robust instruction tuning.

Qualitative analysis. Figure 7 shows responses of clean queries and their visually or textually perturbed counterparts. Although the query before and after each perturbation conveys the same meaning and intention, LLaVA-v1.5 reveals volatility in its responses, whereas Vittle shows stable behavior by providing consistent responses, i.e., generating exactly the same response in the case of visual perturbation while keep focusing on the same object in a case of textual perturbation.

Representation analysis. We next see how Vittle shapes the representation space and how it affects robustness. In Table 4, we measure the average value of empirical JSD and EMID discussed in Section 3.4 over 27 perturbed variants of LB-COCO. Both JSD and EMID are computed between two distributions, clean and one of its perturbed versions, and then averaged over 27 clean-perturbed pairs (See Appendix A.4 for details). As our hypothesis, Vittle reduces distributional gaps, e.g., achieving smaller JSDs, between clean and perturbed samples in its representation space, thereby achieving a smaller EMID value that indicates better robustness. In Figure 8 (top), we further show

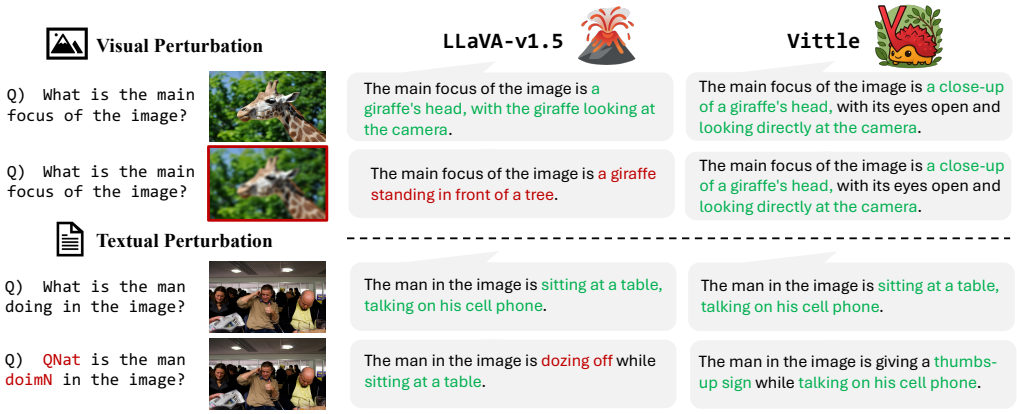

Figure 7: **Case study on LB-COCO under perturbations.** Although LLaVA-v1.5 produces a reasonable response for clean samples, the response and its quality vary under perturbations. `Vittle` maintains the consistency for the responses.

Table 4: **JSD and EMID evaluation on 27 LB-COCO variants.** We measure JSD and EMID between clean and perturbed LB-COCO in a pair-wise manner, then report the average value.

Method	JSD (↓)	EMID (↓)
Baseline	0.068	0.026
`Vittle` (L)	0.048	0.021
`Vittle` (F)	0.047	0.025

PCA visualizations (in the same axis scale) for representations of LLaVA and `Vittle` on clean and image-text perturbed LB-COCO. We see that `Vittle` embeds the clean and semantically equivalent perturbed samples more closely. Moreover, the bottom panel shows that `Vittle` induces smaller cosine distances between clean and perturbed pairs in terms of the histogram and the average value in parentheses. These results indicate that our learning objective is indeed effective in structuring a better representation space that drives robustness.

Table 5: **Runtime comparison.**

Method	Tr./it. (s)	Tr. (h)	Te. (s)
Baseline	7.363	11.06	0.1048
`Vittle`	9.482	13.36	0.1072

Cost analysis. `Vittle` introduces a lightweight bottleneck layer inside of LLM that slightly increases the total number of trainable parameters (by 1.5%). One may thus wonder how `Vittle`'s training and inference time is compared with a bottleneck-free baseline. In Table 5, we show the wall-clock training (per iter and total), and inference time per sample. Although `Vittle` increases the training time up to 20% compared with baseline, *its inference time is almost identical to the original model*, which is a reasonable cost given significant gains in terms of robustness.

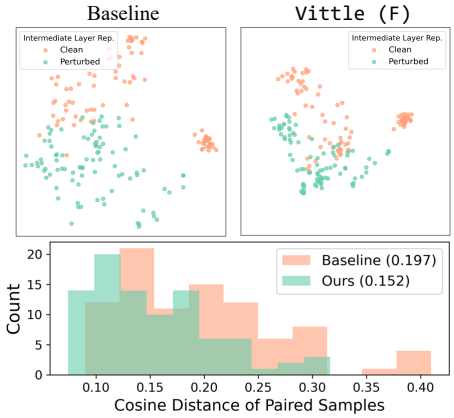

Figure 8: **PCA and pair-wise cosine distance of representations between clean and perturbed samples.** Results on the joint perturbation (Zoom Blur with Arabic translation) show that `Vittle` induces better invariance.

5. Conclusion

This work provided the first investigation on the promise of information bottleneck from the context of MLLM instruction tuning to ensure robustness of MLLM under distribution shifts. We proposed a new theoretically-grounded visual instruction tuning method, `Vittle`, that injects a bottleneck layer inside the LLM to induce posterior samples of internal representations that encode useful information to produce valid responses while discarding other residual information from input queries. With negligible additional cost, `Vittle` is easily optimized with a variational lower bound of IB and shows consistent gains in robustness in 30 types of distribution shifts while also achieving strong performance on standard benchmarks, indicating that `Vittle` promotes a good balance between invariance and sensitivity during representation learning.

References

Achille, A. and Soatto, S. Information dropout: Learning optimal representations through noisy computation. *IEEE Transactions on Pattern Analysis and Machine Intelligence*, 40(12):2897–2905, 2018. doi: 10.1109/TPAMI.2017.2784440.

Alemi, A. A., Fischer, I., Dillon, J. V., and Murphy, K. Deep variational information bottleneck. In *International Conference on Learning Representations*, 2017.

AlSaad, R., Abd-Alrazaq, A., Boughorbel, S., Ahmed, A., Renault, M.-A., Damseh, R., and Sheikh, J. Multimodal large language models in health care: Applications, challenges, and future outlook. *J. Med. Internet Res.*, 26: e59505, 2024.

Arora, S., Ge, R., Neyshabur, B., and Zhang, Y. Stronger generalization bounds for deep nets via a compression approach. In *International conference on machine learning*, pp. 254–263. PMLR, 2018.

Bai, J., Guo, H., Peng, Z., Yang, J., Li, Z., Li, M., and Tian, Z. Mitigating hallucinations in large vision-language models by adaptively constraining information flow. In *Proceedings of the AAAI Conference on Artificial Intelligence*, volume 39, pp. 23442–23450, 2025a.

Bai, S., Chen, K., Liu, X., Wang, J., Ge, W., Song, S., Dang, K., Wang, P., Wang, S., Tang, J., et al. Qwen2.5-vl technical report. *arXiv preprint arXiv:2502.13923*, 2025b.

Barlow, H. B. et al. Possible principles underlying the transformation of sensory messages. *Sensory communication*, 1(01):217–233, 1961.

Blei, D. M., Kucukelbir, A., and and, J. D. M. Variational inference: A review for statisticians. *Journal of the American Statistical Association*, 112(518):859–877, 2017. doi: 10.1080/01621459.2017.1285773. URL https://doi.org/10.1080/01621459.2017.1285773.

Blumer, A., Ehrenfeucht, A., Haussler, D., and Warmuth, M. K. Occam's razor. *Information Processing Letters*, 24 (6):377–380, 1987. ISSN 0020-0190.

Caffagni, D., Cocchi, F., Barsellotti, L., Moratelli, N., Sarto, S., Baraldi, L., Cornia, M., and Cucchiara, R. The revolution of multimodal large language models: A survey. In *Findings of the Association for Computational Linguistics: ACL 2024*, pp. 13590–13618, 2024.

Chen, K., Zhang, Z., Zeng, W., Zhang, R., Zhu, F., and Zhao, R. Shikra: Unleashing multimodal llm's referential dialogue magic. *arXiv preprint arXiv:2306.15195*, 2023.

Chen, L., Li, J., Dong, X., Zhang, P., Zang, Y., Chen, Z., Duan, H., Wang, J., Qiao, Y., Lin, D., and Zhao, F. Are we on the right way for evaluating large vision-language models? In *The Thirty-eighth Annual Conference on Neural Information Processing Systems*, 2024a. URL https://openreview.net/forum?id=evP9mxNNxJ.

Chen, Z., Wang, W., Cao, Y., Liu, Y., Gao, Z., Cui, E., Zhu, J., Ye, S., Tian, H., Liu, Z., et al. Expanding performance boundaries of open-source multimodal models with model, data, and test-time scaling. *arXiv preprint arXiv:2412.05271*, 2024b.

Cheng, P., Hao, W., Dai, S., Liu, J., Gan, Z., and Carin, L. Club: A contrastive log-ratio upper bound of mutual information. In *International conference on machine learning*, pp. 1779–1788. PMLR, 2020.

Chiang, W.-L., Li, Z., Lin, Z., Sheng, Y., Wu, Z., Zhang, H., Zheng, L., Zhuang, S., Zhuang, Y., Gonzalez, J. E., Stoica, I., and Xing, E. P. Vicuna: An open-source chatbot impressing gpt-4 with 90%* chatgpt quality, March 2023. URL https://lmsys.org/blog/2023-03-30-vicuna/.

Chun, S., Oh, S. J., De Rezende, R. S., Kalantidis, Y., and Larlus, D. Probabilistic embeddings for cross-modal retrieval. In *Proceedings of the IEEE/CVF conference on computer vision and pattern recognition*, pp. 8415–8424, 2021.

Conneau, A. Unsupervised cross-lingual representation learning at scale. *arXiv preprint arXiv:1911.02116*, 2019.

Cover, T. M. *Elements of information theory*. John Wiley & Sons, 1999.

Cui, C., Ma, Y., Cao, X., Ye, W., Zhou, Y., Liang, K., Chen, J., Lu, J., Yang, Z., Liao, K.-D., Gao, T., Li, E., Tang, K., Cao, Z., Zhou, T., Liu, A., Yan, X., Mei, S., Cao, J., Wang, Z., and Zheng, C. A survey on multimodal large language models for autonomous driving. In *Proceedings of the IEEE/CVF Winter Conference on Applications of Computer Vision (WACV) Workshops*, pp. 958–979, January 2024a.

Cui, X., Aparcedo, A., Jang, Y. K., and Lim, S.-N. On the robustness of large multimodal models against image adversarial attacks. In *Proceedings of the IEEE/CVF Conference on Computer Vision and Pattern Recognition*, pp. 24625–24634, 2024b.

Dai, W., Li, J., LI, D., Tiong, A., Zhao, J., Wang, W., Li, B., Fung, P. N., and Hoi, S. Instructblip: Towards general-purpose vision-language models with instruction tuning. *Advances in Neural Information Processing Systems*, 36: 49250–49267, 2023.

Du, Y., Xu, J., Xiong, H., Qiu, Q., Zhen, X., Snoek, C. G., and Shao, L. Learning to learn with variational information bottleneck for domain generalization. In *Computer Vision–ECCV 2020: 16th European Conference, Glasgow, UK, August 23–28, 2020, Proceedings, Part X 16*, pp. 200–216. Springer, 2020.

Esser, P., Rombach, R., and Ommer, B. Taming transformers for high-resolution image synthesis. In *Proceedings of the IEEE/CVF conference on computer vision and pattern recognition*, pp. 12873–12883, 2021.

Federici, M., Dutta, A., Forré, P., Kushman, N., and Akata, Z. Learning robust representations via multi-view information bottleneck. In *International Conference on Learning Representations*, 2020. URL https://openreview.net/forum?id=B1xwcyHFDr.

Finzi, M., Benton, G., and Wilson, A. G. Residual pathway priors for soft equivariance constraints. *Advances in Neural Information Processing Systems*, 34:30037–30049, 2021.

Geirhos, R., Jacobsen, J.-H., Michaelis, C., Zemel, R., Brendel, W., Bethge, M., and Wichmann, F. A. Shortcut learning in deep neural networks. *Nature Machine Intelligence*, 2(11):665–673, 2020.

Google Cloud. Gemini 2.5 Pro. https://cloud.google.com/vertex-ai/generative-ai/docs/models/gemini/2-5-pro?hl=ko, May 2025.

Goyal, S., Kumar, A., Garg, S., Kolter, Z., and Raghunathan, A. Finetune like you pretrain: Improved finetuning of zero-shot vision models. In *Proceedings of the IEEE/CVF Conference on Computer Vision and Pattern Recognition*, pp. 19338–19347, 2023.

Graves, A. Practical variational inference for neural networks. *Advances in neural information processing systems*, 24, 2011.

Gray, E. and Tall, D. Abstraction as a natural process of mental compression. *Mathematics Education Research Journal*, 19(2):23–40, 2007.

Groot, T. and Valdenegro-Toro, M. Overconfidence is key: Verbalized uncertainty evaluation in large language and vision-language models. In *Proceedings of the 4th Workshop on Trustworthy Natural Language Processing (TrustNLP 2024)*, pp. 145–171, 2024.

Grünwald, P. Minimum description length tutorial. *Advances in minimum description length: Theory and applications*, 5:1–80, 2005.

Gu, S., Zhang, J., Zhou, S., Yu, K., Xing, Z., Wang, L., Cao, Z., Jia, J., Zhang, Z., Wang, Y., et al. Infinity-mm: Scaling multimodal performance with large-scale and high-quality instruction data. *arXiv preprint arXiv:2410.18558*, 2024.

Han, W., Chen, H., and Poria, S. Towards robust instruction tuning on multimodal large language models. *arXiv preprint arXiv:2402.14492*, 2024a.

Han, Z., Zhou, G., He, R., Wang, J., Wu, T., Yin, Y., Khan, S., Yao, L., Liu, T., and Zhang, K. How well does gpt-4v (ision) adapt to distribution shifts? a preliminary investigation. In *ICLR 2024 Workshop on Mathematical and Empirical Understanding of Foundation Models*, 2024b.

Hernandez, E. and Andreas, J. The low-dimensional linear geometry of contextualized word representations. In *Proceedings of the 25th Conference on Computational Natural Language Learning*, pp. 82–93, 2021.

Hinton, G. E. and Van Camp, D. Keeping the neural networks simple by minimizing the description length of the weights. In *Proceedings of the sixth annual conference on Computational learning theory*, pp. 5–13, 1993.

Hoyos-Osorio, J. K. and Sanchez-Giraldo, L. G. The representation jensen-shannon divergence. *arXiv preprint arXiv:2305.16446*, 2023.

Hu, E. J., yelong shen, Wallis, P., Allen-Zhu, Z., Li, Y., Wang, S., Wang, L., and Chen, W. LoRA: Low-rank adaptation of large language models. In *International Conference on Learning Representations*, 2022. URL https://openreview.net/forum?id=nZeVKeeFYf9.

Hwang, J., Cheung, B., Hong, Z.-W., Boopathy, A., Agrawal, P., and Fiete, I. Imagenet-rib benchmark: Large pre-training datasets don't guarantee robustness after fine-tuning. *arXiv preprint arXiv:2410.21582*, 2024.

Karamcheti, S., Nair, S., Balakrishna, A., Liang, P., Kollar, T., and Sadigh, D. Prismatic vlms: Investigating the design space of visually-conditioned language models. In *Forty-first International Conference on Machine Learning*, 2024.

Kawaguchi, K., Deng, Z., Ji, X., and Huang, J. How does information bottleneck help deep learning? In *International Conference on Machine Learning*, pp. 16049–16096. PMLR, 2023.

Kingma, D. P. and Welling, M. Auto-encoding variational bayes. In *International Conference on Learning Representations (ICLR)*, 2014.

Kumar, A., Raghunathan, A., Jones, R., Ma, T., and Liang, P. Fine-tuning can distort pretrained features and underperform out-of-distribution. In *International Conference on Learning Representations*, 2022.

Lee, T., Tu, H., Wong, C. H., Zheng, W., Zhou, Y., Mai, Y., Roberts, J., Yasunaga, M., Yao, H., Xie, C., et al. Vhelm: A holistic evaluation of vision language models. *Advances in Neural Information Processing Systems*, 37: 140632–140666, 2024.

Lee, Y., Chen, A. S., Tajwar, F., Kumar, A., Yao, H., Liang, P., and Finn, C. Surgical fine-tuning improves adaptation to distribution shifts. In *The Eleventh International Conference on Learning Representations*, 2023. URL https://openreview.net/forum?id=APuPRxjHvZ.

Li, B., Shen, Y., Wang, Y., Zhu, W., Li, D., Keutzer, K., and Zhao, H. Invariant information bottleneck for domain generalization. In *Proceedings of the AAAI Conference on Artificial Intelligence*, volume 36, pp. 7399–7407, 2022a.

Li, B., Zhang, K., Zhang, H., Guo, D., Zhang, R., Li, F., Zhang, Y., Liu, Z., and Li, C. Llava-next: Stronger llms supercharge multimodal capabilities in the wild, May 2024a. URL https://llava-vl.github.io/blog/2024-05-10-llava-next-stronger-llms/.

Li, B., Zhang, Y., Guo, D., Zhang, R., Li, F., Zhang, H., Zhang, K., Zhang, P., Li, Y., Liu, Z., et al. Llava-onevision: Easy visual task transfer. *arXiv preprint arXiv:2408.03326*, 2024b.

Li, J., Li, D., Xiong, C., and Hoi, S. Blip: Bootstrapping language-image pre-training for unified vision-language understanding and generation. In *International conference on machine learning*, pp. 12888–12900. PMLR, 2022b.

Li, X., Wen, C., Hu, Y., Yuan, Z., and Zhu, X. X. Vision-language models in remote sensing: Current progress and future trends. *IEEE Geoscience and Remote Sensing Magazine*, 2024c.

Li, Y., Du, Y., Zhou, K., Wang, J., Zhao, W. X., and Wen, J.-R. Evaluating object hallucination in large vision-language models. In *Proceedings of the 2023 Conference on Empirical Methods in Natural Language Processing*, pp. 292–305, 2023.

Li, Y., Zhao, H., Jiang, H., Pan, Y., Liu, Z., Wu, Z., Shu, P., Tian, J., Yang, T., Xu, S., et al. Large language models for manufacturing. *arXiv preprint arXiv:2410.21418*, 2024d.

Li, Y., Rügamer, D., Bischl, B., and Rezaei, M. Calibrating LLMs with information-theoretic evidential deep learning. In *The Thirteenth International Conference on Learning Representations*, 2025. URL https://openreview.net/forum?id=YcML3rJl0N.

Liang, Y., Zheng, T., Du, X., Zhang, G., Liu, J., Qu, X., Zu, W., Xing, X., Zheng, C., Ma, L., et al. Aligning instruction tuning with pre-training. *arXiv preprint arXiv:2501.09368*, 2025.

Liang, Z., Xu, Y., Hong, Y., Shang, P., Wang, Q., Fu, Q., and Liu, K. A survey of multimodel large language models. In *Proceedings of the 3rd International Conference on Computer, Artificial Intelligence and Control Engineering*, pp. 405–409, 2024.

Lin, T.-Y., Maire, M., Belongie, S., Hays, J., Perona, P., Ramanan, D., Dollár, P., and Zitnick, C. L. Microsoft coco: Common objects in context. In *Computer vision–ECCV 2014: 13th European conference, zurich, Switzerland, September 6-12, 2014, proceedings, part v 13*, pp. 740–755. Springer, 2014.

Littlestone, N. and Warmuth, M. Relating data compression and learnability. *Unpublished notes*, 1986.

Liu, F., Lin, K., Li, L., Wang, J., Yacoob, Y., and Wang, L. Mitigating hallucination in large multi-modal models via robust instruction tuning. In *The Twelfth International Conference on Learning Representations*, 2024a. URL https://openreview.net/forum?id=J44HfH4JCg.

Liu, H., Li, C., Wu, Q., and Lee, Y. J. Visual instruction tuning. *Advances in neural information processing systems*, 36:34892–34916, 2023.

Liu, H., Li, C., Li, Y., and Lee, Y. J. Improved baselines with visual instruction tuning. In *Proceedings of the IEEE/CVF Conference on Computer Vision and Pattern Recognition*, pp. 26296–26306, 2024b.

Liu, H., Li, C., Li, Y., Li, B., Zhang, Y., Shen, S., and Lee, Y. J. Llava-next: Improved reasoning, ocr, and world knowledge, January 2024c. URL https://llava-vl.github.io/blog/2024-01-30-llava-next/.

Liu, S., Ye, H., and Zou, J. Reducing hallucinations in large vision-language models via latent space steering. In *The Thirteenth International Conference on Learning Representations*, 2025. URL https://openreview.net/forum?id=LBl7Hez0fF.

Liu, Z., Wang, T., Shi, J., Zheng, X., Chen, Z., Song, L., Dong, W., Obeysekera, J., Shirani, F., and Luo, D.

Timex++: Learning time-series explanations with information bottleneck. In *International Conference on Machine Learning*, pp. 32062–32082. PMLR, 2024d.

Lu, P., Mishra, S., Xia, T., Qiu, L., Chang, K.-W., Zhu, S.-C., Tafjord, O., Clark, P., and Kalyan, A. Learn to explain: Multimodal reasoning via thought chains for science question answering. *Advances in Neural Information Processing Systems*, 35:2507–2521, 2022.

Lu, Y., Jiang, D., Chen, W., Wang, W. Y., Choi, Y., and Lin, B. Y. Wildvision: Evaluating vision-language models in the wild with human preferences. In *The Thirty-eight Conference on Neural Information Processing Systems Datasets and Benchmarks Track*, 2024. URL https://openreview.net/forum?id=i92eyFCQHC.

Luo, Y., Liu, P., Guan, T., Yu, J., and Yang, Y. Significance-aware information bottleneck for domain adaptive semantic segmentation. In *Proceedings of the IEEE/CVF international conference on computer vision*, pp. 6778–6787, 2019.

Mahabadi, R. K., Belinkov, Y., and Henderson, J. Variational information bottleneck for effective low-resource fine-tuning. *arXiv preprint arXiv:2106.05469*, 2021.

Miao, S., Liu, M., and Li, P. Interpretable and generalizable graph learning via stochastic attention mechanism. In *International Conference on Machine Learning*, pp. 15524–15543. PMLR, 2022.

Miller, G. A. The magical number seven, plus or minus two: Some limits on our capacity for processing information. *Psychological review*, 63(2):81, 1956.

Oh, C., Kim, M., Lim, H., Park, J., Jeong, E., Cheng, Z.-Q., and Song, K. Towards calibrated robust fine-tuning of vision-language models. *Advances in Neural Information Processing Systems*, 37, 2024.

Oh, C., Fang, Z., Im, S., Du, X., and Li, Y. Understanding multimodal llms under distribution shifts: An information-theoretic approach. In *International Conference on Machine Learning*, 2025a.

Oh, C., Li, Y., Song, K., Yun, S., and Han, D. Dawin: Training-free dynamic weight interpolation for robust adaptation. In *The Thirteenth International Conference on Learning Representations*, 2025b. URL https://openreview.net/forum?id=L8e7tBf4pP.

Oh, S. J., Gallagher, A. C., Murphy, K. P., Schroff, F., Pan, J., and Roth, J. Modeling uncertainty with hedged instance embeddings. In *International Conference on Learning Representations*, 2019. URL https://openreview.net/forum?id=r1xQQhAqKX.

OpenAI. OpenAI o3 and o4-mini System Card. https://openai.com/index/o3-o4-mini-system-card/, April 2025.

Oquab, M., Darcet, T., Moutakanni, T., Vo, H. V., Szafraniec, M., Khalidov, V., Fernandez, P., HAZIZA, D., Massa, F., El-Nouby, A., Assran, M., Ballas, N., Galuba, W., Howes, R., Huang, P.-Y., Li, S.-W., Misra, I., Rabbat, M., Sharma, V., Synnaeve, G., Xu, H., Jegou, H., Mairal, J., Labatut, P., Joulin, A., and Bojanowski, P. DINOv2: Learning robust visual features without supervision. *Transactions on Machine Learning Research*, 2024. ISSN 2835-8856. URL https://openreview.net/forum?id=a68SUt6zFt. Featured Certification.

Ordonez, V., Kulkarni, G., and Berg, T. Im2text: Describing images using 1 million captioned photographs. *Advances in neural information processing systems*, 24, 2011.

Qiu, J., Zhu, Y., Shi, X., Wenzel, F., Tang, Z., Zhao, D., Li, B., and Li, M. Benchmarking robustness of multimodal image-text models under distribution shift. *Journal of Data-centric Machine Learning Research*, 2024. URL https://openreview.net/forum?id=Vc1fXQ8mJg.

Radford, A., Kim, J. W., Hallacy, C., Ramesh, A., Goh, G., Agarwal, S., Sastry, G., Askell, A., Mishkin, P., Clark, J., et al. Learning transferable visual models from natural language supervision. In *International conference on machine learning*, pp. 8748–8763. PmLR, 2021.

Rahmanzadehgervi, P., Bolton, L., Taesiri, M. R., and Nguyen, A. T. Vision language models are blind. In *Proceedings of the Asian Conference on Computer Vision*, pp. 18–34, 2024.

Raza, M., Jahangir, Z., Riaz, M. B., Saeed, M. J., and Sattar, M. A. Industrial applications of large language models. *Scientific Reports*, 15(1):13755, 2025.

Rissanen, J. Modeling by shortest data description. *Automatica*, 14(5):465–471, 1978. ISSN 0005-1098.

Rosch, E. Cognitive representations of semantic categories. *Journal of experimental psychology: General*, 104(3): 192, 1975.

Schuhmann, C., Vencu, R., Beaumont, R., Kaczmarczyk, R., Mullis, C., Katta, A., Coombes, T., Jitsev, J., and Komatsuzaki, A. Laion-400m: Open dataset of clip-filtered 400 million image-text pairs. *arXiv preprint arXiv:2111.02114*, 2021.

Sefidgaran, M., Zaidi, A., and Krasnowski, P. Minimum description length and generalization guarantees for representation learning. *Advances in Neural Information Processing Systems*, 36:1489–1525, 2023.

Sharma, P., Ding, N., Goodman, S., and Soricut, R. Conceptual captions: A cleaned, hypernymed, image alt-text dataset for automatic image captioning. In Gurevych, I. and Miyao, Y. (eds.), *Proceedings of the 56th Annual Meeting of the Association for Computational Linguistics (Volume 1: Long Papers)*, pp. 2556–2565, Melbourne, Australia, July 2018. Association for Computational Linguistics. doi: 10.18653/v1/P18-1238. URL https://aclanthology.org/P18-1238/.

Shen, Y., Fu, C., Dong, S., Wang, X., Chen, P., Zhang, M., Cao, H., Li, K., Zheng, X., Zhang, Y., et al. Longvita: Scaling large multi-modal models to 1 million tokens with leading short-context accuray. *arXiv preprint arXiv:2502.05177*, 2025.

Shi, M., Liu, F., Wang, S., Liao, S., Radhakrishnan, S., Zhao, Y., Huang, D.-A., Yin, H., Sapra, K., Yacoob, Y., Shi, H., Catanzaro, B., Tao, A., Kautz, J., Yu, Z., and Liu, G. Eagle: Exploring the design space for multimodal LLMs with mixture of encoders. In *The Thirteenth International Conference on Learning Representations*, 2025. URL https://openreview.net/forum?id=Y2RW9EVwhT.

Shui, C., Chen, Q., Wen, J., Zhou, F., Gagné, C., and Wang, B. A novel domain adaptation theory with jensen–shannon divergence. *Knowledge-Based Systems*, 257: 109808, 2022.

Skean, O., Arefin, M. R., Zhao, D., Patel, N., Naghiyev, J., LeCun, Y., and Shwartz-Ziv, R. Layer by layer: Uncovering hidden representations in language models. *arXiv preprint arXiv:2502.02013*, 2025.

Song, Z.-Y., Li, Z., Cao, Q.-H., Luo, M.-x., and Zhu, H. X. Bridging the dimensional chasm: Uncover layer-wise dimensional reduction in transformers through token correlation. *arXiv preprint arXiv:2503.22547*, 2025.

Tian, J., He, Z., Dai, X., Ma, C.-Y., Liu, Y.-C., and Kira, Z. Trainable projected gradient method for robust fine-tuning. In *Proceedings of the IEEE/CVF Conference on Computer Vision and Pattern Recognition*, pp. 7836–7845, 2023.

Tishby, N. and Zaslavsky, N. Deep learning and the information bottleneck principle. In *2015 ieee information theory workshop (itw)*, pp. 1–5. Ieee, 2015.

Tishby, N., Pereira, F. C., and Bialek, W. The information bottleneck method. *arXiv preprint physics/0004057*, 2000.

Tong, P., Brown, E., Wu, P., Woo, S., IYER, A. J. V., Akula, S. C., Yang, S., Yang, J., Middepogu, M., Wang, Z., et al. Cambrian-1: A fully open, vision-centric exploration of multimodal llms. *Advances in Neural Information Processing Systems*, 37:87310–87356, 2024a.

Tong, S., Liu, Z., Zhai, Y., Ma, Y., LeCun, Y., and Xie, S. Eyes wide shut? exploring the visual shortcomings of multimodal llms. In *Proceedings of the IEEE/CVF Conference on Computer Vision and Pattern Recognition*, pp. 9568–9578, 2024b.

Turner, M. The art of compression. *The artful mind: Cognitive science and the riddle of human creativity*, pp. 93–114, 2006.

Vaswani, A., Shazeer, N., Parmar, N., Uszkoreit, J., Jones, L., Gomez, A. N., Kaiser, Ł., and Polosukhin, I. Attention is all you need. *Advances in neural information processing systems*, 30, 2017.

Vera, M., Piantanida, P., and Vega, L. R. The role of the information bottleneck in representation learning. In *2018 IEEE International Symposium on Information Theory (ISIT)*, pp. 1580–1584, 2018. doi: 10.1109/ISIT.2018.8437679.

Verma, A. A., Saeidi, A., Hegde, S., Therala, A., Bardoliya, F. D., Machavarapu, N., Ravindhiran, S. A. K., Malyala, S., Chatterjee, A., Yang, Y., et al. Evaluating multimodal large language models across distribution shifts and augmentations. In *Proceedings of the IEEE/CVF Conference on Computer Vision and Pattern Recognition*, pp. 5314–5324, 2024.

Wang, H., Zheng, A., Zhao, Y., Wang, T., Ge, Z., Zhang, X., and Zhang, Z. Reconstructive visual instruction tuning. In *The Thirteenth International Conference on Learning Representations*, 2025. URL https://openreview.net/forum?id=8q9NOMzRDg.

Wang, Z., Jian, T., Masoomi, A., Ioannidis, S., and Dy, J. Revisiting hilbert-schmidt information bottleneck for adversarial robustness. *Advances in Neural Information Processing Systems*, 34:586–597, 2021.

Wen, B., Xu, C., Wolfe, R., Wang, L. L., Howe, B., et al. Mitigating overconfidence in large language models: A behavioral lens on confidence estimation and calibration. In *NeurIPS 2024 Workshop on Behavioral Machine Learning*, 2024.

Wilson, A. G. Deep learning is not so mysterious or different. *arXiv preprint arXiv:2503.02113*, 2025.

Wortsman, M., Ilharco, G., Kim, J. W., Li, M., Kornblith, S., Roelofs, R., Lopes, R. G., Hajishirzi, H., Farhadi, A., Namkoong, H., et al. Robust fine-tuning of zero-shot models. In *Proceedings of the IEEE/CVF conference on computer vision and pattern recognition*, pp. 7959–7971, 2022.

Wu, T., Ren, H., Li, P., and Leskovec, J. Graph information bottleneck. *Advances in Neural Information Processing Systems*, 33:20437–20448, 2020.

xAI. Grok 3 Beta — The Age of Reasoning Agents. https://x.ai/news/grok-3, February 2025.

Yang, H., Wang, Y., Xu, X., Zhang, H., and Bian, Y. Can we trust llms? mitigate overconfidence bias in llms through knowledge transfer. *arXiv preprint arXiv:2405.16856*, 2024a.

Yang, H., Zhao, Y., Wu, Y., Wang, S., Zheng, T., Zhang, H., Ma, Z., Che, W., and Qin, B. Large language models meet text-centric multimodal sentiment analysis: A survey. *arXiv preprint arXiv:2406.08068*, 2024b.

Ye, Q., Xu, H., Xu, G., Ye, J., Yan, M., Zhou, Y., Wang, J., Hu, A., Shi, P., Shi, Y., et al. mplug-owl: Modularization empowers large language models with multimodality. *arXiv preprint arXiv:2304.14178*, 2023.

Ye, W., Zheng, G., Ma, Y., Cao, X., Lai, B., Rehg, J. M., and Zhang, A. MM-spubench: Towards better understanding of spurious biases in multimodal LLMs. In *Workshop on Responsibly Building the Next Generation of Multimodal Foundational Models*, 2024. URL https://openreview.net/forum?id=htCZ3fEdV7.

Ye-Bin, M., Hyeon-Woo, N., Choi, W., and Oh, T.-H. Beaf: Observing before-after changes to evaluate hallucination in vision-language models. In *European Conference on Computer Vision*, pp. 232–248. Springer, 2025.

Yeh, M.-H., Wang, J., Du, X., Park, S., Tao, L., Im, S., and Li, Y. Position: Challenges and future directions of data-centric ai alignment. 2025.

Yue, X., Ni, Y., Zhang, K., Zheng, T., Liu, R., Zhang, G., Stevens, S., Jiang, D., Ren, W., Sun, Y., et al. Mmmu: A massive multi-discipline multimodal understanding and reasoning benchmark for expert agi. In *Proceedings of the IEEE/CVF Conference on Computer Vision and Pattern Recognition*, pp. 9556–9567, 2024.

Zhai, X., Mustafa, B., Kolesnikov, A., and Beyer, L. Sigmoid loss for language image pre-training. In *Proceedings of the IEEE/CVF international conference on computer vision*, pp. 11975–11986, 2023.

Zhang, J., Zhang, X.-Y., Wang, C., and Liu, C.-L. Deep representation learning for domain generalization with information bottleneck principle. *Pattern Recognition*, 143:109737, 2023. ISSN 0031-3203.

Zhang, X., Li, J., Chu, W., Hai, J., Xu, R., Yang, Y., Guan, S., Xu, J., and Cui, P. On the out-of-distribution generalization of multimodal large language models. *arXiv preprint arXiv:2402.06599*, 2024.

Zhao, B., Wu, B., He, M., and Huang, T. Svit: Scaling up visual instruction tuning. *arXiv preprint arXiv:2307.04087*, 2023.

Zhaoping, L. Vision: looking and seeing through our brain's information bottleneck. *arXiv preprint arXiv:2503.18804*, 2025.

Zheng, L., Chiang, W.-L., Sheng, Y., Zhuang, S., Wu, Z., Zhuang, Y., Lin, Z., Li, Z., Li, D., Xing, E., et al. Judging llm-as-a-judge with mt-bench and chatbot arena. *Advances in Neural Information Processing Systems*, 36: 46595–46623, 2023.

Zhou, Z., Hong, F., Luo, J., Yao, J., Li, D., Han, B., Zhang, Y., and Wang, Y. Learning to instruct for visual instruction tuning. *arXiv preprint arXiv:2503.22215*, 2025.

Zou, A., Phan, L., Chen, S., Campbell, J., Guo, P., Ren, R., Pan, A., Yin, X., Mazeika, M., Dombrowski, A.-K., et al. Representation engineering: A top-down approach to ai transparency. *arXiv preprint arXiv:2310.01405*, 2023.

Appendix

Contents

1 Introduction **1**

2 Background, Related Work, and Motivation **2**

3 Method **3**

3.1 Preliminary: Information Bottleneck As a Learning Objective . . . 3

3.2 Variational Inference for Information Bottleneck in MLLMs . . . 3

3.3 `Vittle`: A Practical Implementation of Visual Instruction Bottleneck Tuning . . . 4

3.4 Theoretical Justification . . . 5

4 Experiment **6**

4.1 Setup . . . 6

4.2 Results . . . 6

5 Conclusion **9**

A Extended Experiment Setup and Implementation Detail **17**

A.1 Model and Training . . . 17

A.2 `Vittle` Implementation Details . . . 18

A.3 Downstream Task Benchmark Construction . . . 19

A.4 Evaluation Details . . . 21

B Additional Results **22**

B.1 Ablation Study . . . 22

B.2 Full Results of Pair-wise Cosine Distance . . . 24

B.3 Full Results with LLaVA-v1.5-7B and LLaVA-v1.5-13B . . . 24

B.4 Applicability to Other MLLMs . . . 26

C Derivation of Variational Bound for IB in MLLM **28**

D Missing Proof **29**

D.1 Preliminary . . . 29

D.2 A New Upper Bound for Effective Mutual Information Difference . . . 29

E Extended Literature Review **31**

F Limitation and Future Work 32

G Impact Statement 32

A. Extended Experiment Setup and Implementation Detail

A.1. Model and Training

In this work, we consider LLaVA-v1.5 (Liu et al., 2024b) as our target multimodal large language model (MLLM) with CLIP ViT-L/14-336px (Radford et al., 2021) and Vicuna-v1.5-7B (Chiang et al., 2023) as visual encoder and LLM backbone, respectively, and a two-layer MLP as projector (modality connector that maps features of the visual encoder into the text embedding space). Although all of the results presented in the main body of the paper were produced with LLaVA-v1.5-7B, we also experimented with LLaVA-v1.5-13B (with Vicua-v1.5-13B as the LLM backbone) to validate the scalability of our method, and consider Prism-7B (Karamcheti et al., 2024) as an additional MLLM architecture to validate the broad applicability of `Vittle`. For fair comparison, all models are trained on the `LLaVA-pretrain-558k` and `LLaVA-mix-665k` datasets, consisting of a mixture of LAION (Schuhmann et al., 2021), CC (Sharma et al., 2018), SBU (Ordonez et al., 2011) datasets with BLIP captions (Li et al., 2022b) and a mixture of `LLaVA-instruct-158K` and academic-task-oriented (V)QA datasets, respectively. Training configurations such as optimizer, learning rate, and batch size are summarized in Table 6 and Table 7. All training runs are conducted with eight A100-80GB GPUs with DeepSpeed ZeRO library. The shortest run takes roughly 11 hours, whereas the longest run takes about 14 hours. Now, we elaborate on the overall workflow of LLaVA and Prism below.

Table 6: **Hyperparameter list of `Vittle` training.** We adopt exactly the same configurations with LLaVA-v1.5 (Liu et al., 2024b) for Stage 1 and 2.

Config	Stage1	Stage2
Global batch size	256	128
Batch size per GPU	32	16
Learning rate	1e-3	2e-5
Learning rate schedule	Cosine decay w/ linear warmup	
Warmup ratio	0.03	
Weight decay	0.0	
Epoch	1	
Optimizer	AdamW	
Precision	bf16	

Table 7: **Hyperparameter list of `Prism-Vittle` training.** We adopt exactly the same configurations with Prism-DINOSigLIP-Controlled-7B (Karamcheti et al., 2024) single stage training.

Config	Value
Global batch size	128
Batch size per GPU	16
Learning rate	2e-5
Learning rate schedule	cosine decay w/ linear-warmup
Warmup ratio	0.03
Weight decay	0.1
Epoch	1
Optimizer	AdamW
Precision	bf16

LLaVA is built with a pre-trained visual encoder that takes visual inputs, a pre-trained LLM backbone that takes text instructions, and a lightweight projector that maps features produced by the visual encoder into the text embedding space of LLM backbone so that the visually-grounded multimodal instruction input query can be processed by the LLM backbone. LLaVA undergoes a two-stage training: (1) The first stage takes into account modality alignment, where the projector is trained on image and corresponding instruction or caption with a conditional language modeling loss implemented by aggregating cross-entropy losses across response tokens, while the visual encoder and LLM backbone are frozen. (2) The second stage stands for the instruction tuning, where the projector and LLM backbone are jointly trained on multimodal instruction samples with the same conditional language modeling loss while the visual encoder is still frozen. This two-stage training has been considered a standard approach for developing MLLMs and is widely adopted (Chen et al., 2023; Ye et al., 2023; Tong et al., 2024a).

Prism has a model architecture similar to LLaVA, but provides some valuable insight into the design of the MLLM training recipe, and we note two remarkable design choices of Prism that distinguish it from LLaVA: (1) incorporating multiple visual encoders rather than hosting a single visual encoder, and (2) reducing the two-stage alignment-then-instruction tuning into a single-stage instruction tuning. Note that different self-supervised visual representation learning induces features that have different strengths, and several works reveal the benefits of ensembling multiple different visual encoders to leverage complementary advantages (Tong et al., 2024b; Karamcheti et al., 2024; Shi et al., 2025). Prism incorporates SigLIP (Zhai et al., 2023) and DINOv2 (Oquab et al., 2024) to enjoy both a robust global feature and a fine-grained local feature. Meanwhile, Karamcheti et al. (Karamcheti et al., 2024) showed that the simplified single-stage training strategy can be a cost-effective alternative to the standard two-stage training.

To train these MLLMs, we consider five baseline approaches: (1) the standard full LLM fine-tuning with conditional language modeling loss, (2) parameter-efficient LoRA (Hu et al., 2022) fine-tuning with the conditional language modeling loss, (3) conditional language modeling loss with weight decay regularization, (4) reconstructive visual instruction tuning (ROSS) (Wang et al., 2025), and (5) learning to instruct (LIT) (Zhou et al., 2025). For the LoRA-based training configuration, we use the same one provided by the official LLaVA-v1.5 repository[3], and for the weight decay regularization, we select the regularization magnitude parameter among $\{0.1, 0.01, 0.001\}$ based on the POPE evaluation result. We now elucidate two competitive baseline methods, ROSS and LIT, in the following paragraphs. It is worth noting that these methods are designed to encode more (visual) information into the representation space, which is opposite to our `Vittle`'s design motivation that pursues a minimal sufficient representation for improving robustness to distribution shifts.

Reconstructive visual instruction tuning (ROSS) follows the two-stage training of LLaVA, but tries to reconstruct the visual inputs from the LLM backbone by adopting a regression or denoising learning objective in addition to language modeling loss during its second stage. By doing so, ROSS guides the MLLM to learn a much richer visual understanding, which is usually lacking in modern MLLMs (Tong et al., 2024b; Rahmanzadehgervi et al., 2024). The reconstruction target can be a raw RGB pixel value or the latent representation from an external visual encoder such as VQGAN (Esser et al., 2021) or VAE (Kingma & Welling, 2014), and ROSS requires an additional trainable module to reconstruct visual content, which is discarded during inference. We follow the training recipe from the official code repository[4] to replicate ROSS-D-7B with the same visual encoder and LLM backbone to LLaVA-v1.5. For a fair comparison with LLaVA and `Vittle`, we train the ROSS with the same dataset (that of LLaVA-v1.5) for both training stages, while the original ROSS model was trained on a slightly larger dataset in the second stage.

Learning to Instruct (LIT) also focuses on the visual shortcomings of current MLLM and tries to improve the visual understanding capability of MLLM by incorporating an additional loss term that incentivizes the encoding of additional visual information. To be specific, while the cross-entropy loss in LLaVA's conditional language modeling objective is aggregated through the response tokens only, LIT introduces an extra cross-entropy loss term, which is aggregated over the instruction (question) tokens only, thereby enforcing MLLM to learn to predict a proper textual instruction given an image. As LIT uses the same visual and language backbone model and training dataset as LLaVA-v1.5, we use the pre-trained checkpoint of LIT from Hugging Face[5] for evaluation.

In Figure 6, we observe that while ROSS and LIT are somewhat effective in improving performance on object hallucination detection tasks with the aid of enhanced visual understanding capability, they significantly underperform `Vittle` and even the original LLaVA on the open-ended QA task under distribution shifts. This implies that pursuing more information encoding during visual instruction tuning may not result in better robustness to distribution shifts, but aiming to learn a minimal sufficient representation via `Vittle` can be a promising solution for this (See Table 11 for details).

A.2. `Vittle` Implementation Details

This section provides additional details on implementing `Vittle` through Python-style pseudo code in Figure 9 and text below. Following the standard two-stage LLaVA training recipe, we freeze the visual encoder and LLM backbone during the first stage and only train the projector module. In the second stage, `Vittle` inserts a bottleneck layer g_ϕ, consisting of two of the two-layer MLPs $\{g_{\phi_v}, g_{\phi_t}\}$ for visual and textual modalities, inside the LLM backbone to estimate the distributional parameters (mean and diagonal covariance) of the posterior Gaussian distributions for each visual and textual token. Each bottleneck module is constructed with $\{$`nn.Linear(d,d), nn.GELU(), nn.Linear(d,2*d)`$\}$ where `d` denotes the hidden dimension of the LLM backbone, and this results in a slightly increased number of model parameters (up to 1.5% from the baseline). We use these estimated distribution parameters to sample a representation from this posterior via $\tilde{z} = \mu + \sigma \odot \epsilon$ where $\epsilon \sim \mathcal{N}(\mathbf{0}, I)$. Then, for a given bottleneck layer index l and for the maximum length of visual M_v and textual input tokens M_t, the bottleneck layer g_ϕ takes a sequence of token representations $z = \{z_{v,1}, ..., z_{v,M_v}, z_{t,1}, ..., z_{t,M_t}\}$ produced from the layer l to build information-penalized representations $\hat{z} = \{\hat{z}_{v,1}, ..., \hat{z}_{v,M_v}, \tilde{z}_{t,1}, ..., \tilde{z}_{t,M_t}\}$, where $\hat{z} = (1-\alpha)z + \alpha g_\phi(z)$. Here, we use an interpolated representation between the original pre-bottleneck representation z and the post-bottleneck representation $g_\phi(z)$ with an interpolation coefficient α that progressively grows from 0 to 0.5 by a cosine schedule during training. We observe that solely using the post-bottleneck representation induces a diverging language modeling loss at the later steps of training, and speculate that it is hard to generate a valid response with the

[3] https://github.com/haotian-liu/LLaVA
[4] https://github.com/Haochen-Wang409/ross
[5] https://huggingface.co/zhihanzhou/LIT-LLaVA-1.5-Vicuna-7B/tree/main

information-penalized representation only.

Then, we jointly train the LLM backbone, the projector, and this bottleneck layer together during the second stage of training with the objective function 5. As we assume a diagonal covariance Gaussian for the prior and posterior distributions, Kullback–Leibler divergence (KLD) between the prior p and posterior q can be easily expressed as below,

$$D_{\mathrm{KL}}(q,p) = \frac{1}{2}\sum_{j=1}^{d}\big(\log\frac{\sigma_p^2[j]}{\sigma_q^2[j]} - 1 + \frac{(\mu_p[j]-\mu_q[j])^2}{\sigma_p^2[j]} + \frac{\sigma_q^2[j]}{\sigma_p^2[j]}\big) \tag{8}$$

where $\mu_{\cdot}$ and $\sigma_{\cdot}$ denote d-dimensional distributional parameter vectors and $[j]$ indicates j-th element from the vectors. `Vittle` has two important hyperparameters: (1) target layer index l for bottleneck application, and (2) posterior KLD regularization strength parameter β. After tuning across $l \in \{24, 28, 31\}$ and $\beta \in \{\frac{0.01}{d}, \frac{0.05}{d}, \frac{0.1}{d}, \frac{0.2}{d}, \frac{1.0}{d}\}$ where d denotes the latent dimension of the LLM backbone, we set $l = 24$ and $\beta = 0.1/d$ based on the average performance of POPE and LB-COCO clean datasets. The interpolation coefficient α can also be tuned, but we found that increasing α beyond 0.5 hinders stable training and observing increased language modeling loss at the later parts of training progress. Figure 12 and Table 10 present the results of hyperparameter ablation study.

A.3. Downstream Task Benchmark Construction

Open-ended QA task. One of the most representative applications of an MLLM is the generation of free-form responses given multimodal instruction queries. We consider LLaVA-Bench COCO (LB-COCO; (Liu et al., 2023)) as a typical in-distribution (ID) open-ended QA dataset, which is constructed from MS-COCO images (Lin et al., 2014) with GPT-generated text queries that have 90 pairs of image and text. We then generate 27 variants of this LB-COCO by applying nine types of image perturbations, nine types of text perturbations, and nine types of image-text joint perturbations, to benchmark MLLMs' robustness under various distribution shifts (which will be elaborated at the end of this section). Meanwhile, we also consider three datasets LLaVA-Bench in-the-wild (LB-Wild; (Liu et al., 2023)), LLaVA-Bench Wilder (LB-Wilder; (Li et al., 2024a)), and WildVision-Bench (WV-Bench; (Lu et al., 2024)) constructed by real-world web users' image-text paired queries of 60, 128, and 500 samples, respectively, to validate models' capability to address long-tailed queries in practice. This results in 31 different open-ended QA datasets in total: clean and 27 perturbed LB-COCO variants, and three long-tail datasets.

Object hallucination detection task. Meanwhile, one of the most crucial evaluation aspects of an MLLM is the degree of hallucination of its output. A representative benchmark for this is the POPE dataset (Li et al., 2023), where the model is tasked to answer in binary {Yes, No} form given a question about the object's existence given an image. The POPE dataset was also created from the MS-COCO source images with 9,000 corresponding questions, and we consider this dataset as an ID dataset. As we did for the LB-COCO dataset, we generated 9 variants of POPE by applying nine types of visual perturbations to images. Textual perturbations were not considered here because the text query of this dataset is relatively short, so perturbing the core object word token can distort the desired semantics of the question. In summary, we conducted validation on 10 different POPE variants.

Closed-form QA task. There are numerous closed-form QA datasets that assess the internal knowledge of MLLMs from various perspectives. In this paper, we consider four representative datasets: ScienceQA (Lu et al., 2022), MMMU (Yue et al., 2024), MME (Liang et al., 2024), and MMStar (Chen et al., 2024a), which are designed to validate multimodal knowledge and understanding capability across various domains.

Distribution shift simulation. The goal of this study is to improve the robustness of MLLM under distribution shifts. We mainly focus on subtle perturbations on image and text, which is worth-noting problem given the fact that current MLLMs undergo systematic performance degradation under perturbations. We consider nine visual perturbations listed in Table 8, nine textual perturbations listed in Table 9, and nine image-text joint perturbations: {zoom_blur, frost, gaussian_noise} $\times$ {arabic, greek, hindi}. The translations for Arabic, Greek, and Hindi languages from English are conducted by OpenAI GPT-4o with a prompt: "Please translate a {SOURCE} sentence provided by the user into {TARGET}.", and all the remaining perturbations are generated MMRobustness source code[6]. The actual examples of each visual textual perturbation are presented in Figure 11 and Figure 10.

[6] https://github.com/Jielin-Qiu/MM_Robustness

```
def reparam(mu, logvar):
    std = (logvar / 2).exp()
    batch_size, seq_len, hidden_dim = mu.shape
    z = torch.randn(batch_size, seq_len, hidden_dim)
    return mu + std * z

def forward(self, input_embeds, img_seq_len, a, **kwargs):
    ...
    hidden_states = input_embeds
    for l_idx, llm_layer in enumerate(self.llm.layers):
        layer_outputs = llm_layer(hidden_states, **kwargs)
        hidden_states = layer_outputs[0]
        if l_idx == self.bottleneck_layer_idx:
            # posterior inference
            v_params = self.g_v(hidden_states[:,:i_seq_len,:])
            t_params = self.g_t(hidden_states[:,i_seq_len:,:])
            v_mean = v_params[:,:,:self.h_dim]
            v_logvar = v_params[:,:,self.h_dim:]
            t_mean = t_params[:,:,:self.h_dim]
            t_logvar = t_params[:,:,self.h_dim:]
            v_post = reparam(v_mean, v_logvar)
            t_post = reparam(t_mean, t_logvar)
            z_post = torch.cat((v_post, t_post))
            # interpolation between original and bottlenecked
            hidden_states = (1-a) * hidden_states + a * z_post
    ...
```

Listing 1: Forward pass of `Vittle`

```
def normalized_kld(mu, logvar, modality=None):
    if modality is None:
        # vittle (F) - fixed prior N(0,I)
        kl_loss = -0.5 * (1+logvar-mu**2-logvar.exp()).mean()
    else:
        # vittle (L) - learnable prior
        mu_pr, logvar_pr = self.l_prior[modality]
        logvar_d = logvar-logvar_pr
        scaled_mu_d = (mu-mu_pr).pow(2)/logvar_pr.exp()
        var_ratio = logvar.exp()/logvar_pr.exp()
        kl_loss = -0.5 * (1+logvar_d-scaled_mu_d-var_ratio).mean()
    return kl_loss

def loss(self, logits, labels, v_mean, v_logvar, t_mean, t_logvar):
    lm_loss = self.llm.loss_function(logits, labels)
    if self.learnable_prior:
        flag_v, flag_t = "v", "t"
    else:
        flag_v, flag_t = None, None
    kld_v = self.normalized_kld(v_mean, v_logvar, flag_v)
    kld_t = self.normalized_kld(t_mean, t_logvar, flag_t)
    return lm_loss + self.beta * (kld_v + kld_t)
```

Listing 2: Training objective of `Vittle`

Figure 9: PyTorch-style pseudo code for the forward pass and training objective of `Vittle`

Figure 10: **Examples of visual perturbations.**

Table 8: **List of visual perturbations.** We consider nine visual perturbations from four categories: (1) Blur, (2) Digital, (3) Weather, and (4) Noise, to validate the robustness of MLLMs under diverse types of visual perturbations.

Name	Category
Defocus Blur	Blur
Zoom Blur	Blur
Contrast	Digital
Brightness	Weather
Fog	Weather
Frost	Weather
Gaussian Noise	Noise
Shot Noise	Noise
Speckle Noise	Noise

Table 9: **List of textual perturbations.** We consider nine textual perturbations from three categories: (1) character-level, (2) word-level, and (3) sentence-level, to validate the robustness of MLLMs under diverse types of textual perturbations.

Name	Category
Char Typo	Character-level Perturbation
Char Delete	Character-level Perturbation
Char Insert	Character-level Perturbation
Word Swap	Word-level Perturbation
Word Delete	Word-level Perturbation
Word Insert	Word-level Perturbation
Arabic Translation	Sentence-level Perturbation
Greek Translation	Sentence-level Perturbation
Hindi Translation	Sentence-level Perturbation

A.4. Evaluation Details

Open-ended QA task. Compared to multi-choice closed-form QA tasks that have a unique ground-truth answer per question, open-ended free-form generation-style QA tasks do not provide a single ground-truth answer. We follow the current standard evaluation paradigm, (M)LLM-as-a-Judge, that uses an external (usually more powerful) MLLM to gauge the quality of our target MLLM of interest via prompting. To be specific, for a given input query x, reference answer y, MLLM $f_\theta : \mathcal{X} \rightarrow \mathcal{Y}$, and the judge model $r : \mathcal{X} \times \mathcal{Y} \rightarrow \mathbb{Z}^+$, *relative preference* score is defined as, $\mathbb{E}_{x,y}[\frac{r(x,f_\theta(x))}{r(x,y)}]$.

Figure 11: **Examples of textual perturbations.**

For all of our open-ended QA evaluations, we used the same system prompt template provided by LLaVA authors[7], and we also adopted the MS-COCO annotation[8]-based GPT-4 response[9] and the `gpt_answer`[10] released by LLaVA-NeXT authors as reference answers for LB-COCO variants and LB-Wilder, respectively. For LB-Wild and WV-Bench, we generated reference answers with GPT-4o.

Object hallucination detection and closed-form QA task. In contrast to open-ended tasks, all object hallucination detection and closed-form QA tasks provide a single ground truth answer as a form of discrete labels such as {Yes, No} and {A, B, C, D, ...}. For the multi-choice QA datasets, MMMU, MMStar, and ScienceQA, we attached a subfix prompt: "Answer in a character from the given choices directly." at the end of each question for answer formatting, while using the original question text for YES-or-NO datasets, MME and POPE, without a formatting prompt. We measured the exact matching accuracy $\mathbb{E}_{x,y}[\mathbb{I}(_\theta(x) = y)]$ for these tasks.

Effective Mutual Information Difference (EMID) and Jensen-Shannon Divergence (JSD). In addition to the evaluation with traditional metrics, we also consider the EMID and JSD-based evaluation, which was recently proposed as an information-theoretic approach to measure the robustness of MLLMs (Oh et al., 2025a). To compute the empirical estimates of MI, which is required for EMID computation, we use the CLUB estimator (Cheng et al., 2020) and reproduce the training and inference process of (Oh et al., 2025a) by adopting image and text embeddings for the input image and text from CLIP-ViT-B/32 (Radford et al., 2021) and XLM-RoBERTa-Base (Conneau, 2019) to replace X_v and X_t, and also the text embeddings of XLM-RoBERTa-Base for responses Y and Y_Θ. To compute empirical estimates of JSD, we adopted the representation JSD estimator (Hoyos-Osorio & Sanchez-Giraldo, 2023) on top of the CLIP-ViT-B/32 and XLM-RoBERTa-Base, too.

Representation analysis. Inspired by a recent work that reveals the importance of intermediate layer representation of the LLM backbone (Skean et al., 2025), we use the last input token embedding of the 24th layer (out of 32 layers in a 7B LLM backbone) for all experiments carried out in the representation space (Figure 1 (b) right, Figure 8, Figure 13, and the JSD computation in Table 4).

B. Additional Results

B.1. Ablation Study

We first investigate two important hyperparameters for `Vittle`: (1) bottleneck layer index l and (2) KLD regularization strength β, where we determined those parameter values based on the average performance on the clean POPE and LB-

[7] https://github.com/haotian-liu/LLaVA/blob/main/llava/eval/table/rule.json
[8] https://github.com/haotian-liu/LLaVA/blob/main/llava/eval/table/caps_boxes_coco2014_val_80.jsonl
[9] https://github.com/haotian-liu/LLaVA/blob/main/playground/data/coco2014_val_qa_eval/qa90_gpt4_answer.jsonl
[10] https://huggingface.co/datasets/lmms-lab/LLaVA-Bench-Wilder

COCO, while not observing performance on perturbation datasets for fair model selection. We then further explore the impact of the interpolation coefficient α, which plays a role in controlling the balance between the original representation and the bottleneck representation. Note that we could not conduct such an extensive search due to the computational burden of training 7B 13B scale models, so the hyperparameter values found here may not be optimal, and `Vittle` can achieve better results with further hyperparameter tuning.

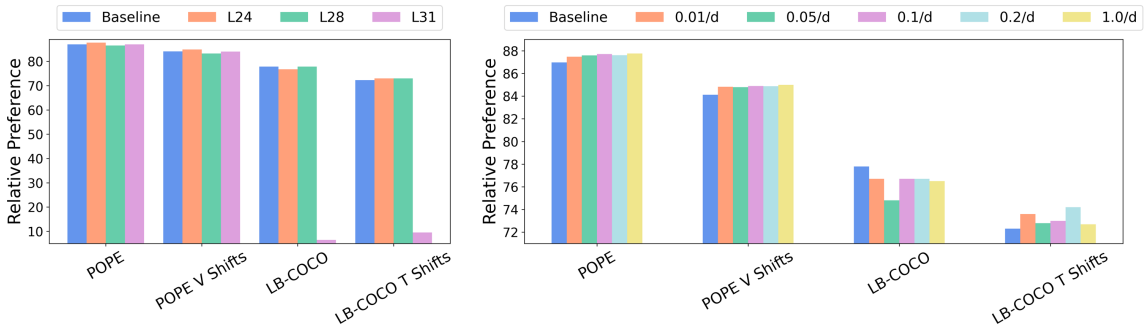

Figure 12: **Ablation study for the bottleneck layer index (left) and KLD regularization magnitude parameter β (right).**

For bottleneck target layer ablation (Figure 12 left), we swept across $\{8, 16, 20, 24, 28, 31\}$ out of 32 layers of the 7B-size LLM backbone. However, applying the bottleneck on the early layer failed to make the language modeling loss converge, so we only provided results for 24, 28, and 31 layers. We observed that intermediate layers (L24 and L28) achieve better results than the penultimate layer (L31), and L24 shows better results on POPE while L28 outperforms L24 on LB-COCO. In conclusion, applying the bottleneck to too early parts hinders shaping some shallow syntactic features that will be actively used at later parts of the layers (Hernandez & Andreas, 2021), whereas applying it to too late parts hurts output-specific alignment or formatting (Song et al., 2025), which guide us to decide intermediate layer, i.e., 24th, as a default choice. This is in line with a recent finding that the intermediate layer of LLM matters more than the early or later layers by showing that the quality measurements of the intermediate layer representations have a stronger correlation with performance in downstream tasks (Skean et al., 2025). Although we can search different layer indices for visual and textual tokens, we leave this to future work.

For KLD regularization strength parameter ablation (Figure 12 right), we swept across $\{0.01, 0.05, 0.1, 0.2, 1.0\}$, and found that in the POPE dataset, strong regularization results in better performance, whereas it is not the case for LB-COCO. We choose $0.1/d$ as our default, which induces balanced clean-data performance on these two tasks.

Table 10: **Ablation study for the representation interpolation coefficient α of the bottleneck layer.** We observe that using the bottlenecked representation beyond the half portion of the total hinders the convergence of the language modeling loss.

Alpha	POPE	POPE V Shifts Avg.	LB-COCO	LB-COCO T Shifts Avg.
Baseline	86.98	84.12	77.8	72.3
0.1	87.22	84.20	**77.9**	**73.1**
0.25	87.34	84.47	75.6	**73.1**
0.5	**87.71**	**84.90**	76.7	73.0
0.75	Failed to converge			
1	Failed to converge			

We also explore the effect of the representation interpolation parameter $\alpha \in [0, 1]$, which can be interpreted as a gating mechanism to control the information flow. As α approaches one, the later parts of the LLM backbone (LLM head in our notation) mainly use the information-penalized representation, while if α becomes smaller, the model strongly relies on the original representation. In Table 10, we observe that using too large values of α results in diverging language modeling loss, indicating that using a strongly penalized representation only cannot predict proper response tokens in sequence. Meanwhile,

Table 11: **Comparison with alternative training approaches.** We compare `Vittle` with weight-space regularization methods, LoRA (Hu et al., 2022) and weight decay (WD), and two recent visual instruction tuning learning objectives, ROSS (Wang et al., 2025) and LIT (Zhou et al., 2025) on LLaVA-v1.5-7B model. Evaluations are conducted on POPE, its nine visually perturbed variants (POPE V Pert.), LB-COCO, and its nine {visually/textually/jointly} perturbed variants, where we mark the best one as bold and the second best one as underlined.

Method	POPE	POPE V Pert.	LB-COCO	LB-COCO V Pert.	LB-COCO T Pert.	LB-COCO J Pert.
Baseline	86.98	84.12	**77.8**	73.4	72.2	62.3
LoRA	83.33	80.23	73.4	70.4	62.7	39.7
WD	87.22	83.97	74.1	72.1	<u>73.0</u>	59.5
ROSS	<u>87.79</u>	84.67	74.4	72.0	71.3	60.0
LIT	87.38	84.21	<u>77.5</u>	72.1	72.9	58.9
`Vittle` (L)	87.71	<u>84.91</u>	76.7	<u>73.9</u>	<u>73.0</u>	<u>62.7</u>
`Vittle` (F)	**87.81**	**84.99**	76.1	**74.2**	**74.1**	**64.4**

Table 12: **`Vittle` on LLaVA-v1.5-13B model.** We compare `Vittle` with the standard learning objective on LLaVA-v1.5-13B model that uses Vicuna-v1.5-13B as an LLM backbone. We set the bottleneck layer index $l = 36$, interpolation coefficient $\alpha = 0.5$, and bottleneck KLD regularization strength $\beta = \frac{0.1}{d}$. `Vittle` outperforms baseline on perturbed datasets while showing rivaling performance on the clean dataset.

Method	POPE	POPE V Pert.	LB-COCO	LB-COCO V Pert.	LB-COCO T Pert.	LB-COCO J Pert.
Baseline	87.14	84.02	**76.9**	73.5	73.8	64.6
`Vittle` (L)	87.22	**84.85**	76.6	**74.5**	**74.0**	**65.4**
`Vittle` (F)	**87.32**	84.65	76.8	74.2	73.9	65.3

the larger value of α induces better POPE performance, whereas the trend is inconsistent in the LB-COCO data set, which is consistent with the observations from the previous ablation study in β.

B.2. Full Results of Pair-wise Cosine Distance

We speculate that the performance degradation of MLLMs under perturbations originates from the representation discrepancy between clean and perturbed samples. That is, in the ideal case, a clean sample and its semantically equivalent perturbed sample should be closely mapped in the representation space, but current MLLMs did not shape the representation space in that way (see Figure 1 and Figure 8). In Figure 13, we provide the histograms of representation space pair-wise cosine distance between clean and perturbed examples in 27 types of perturbations. As we can see, `Vittle` (F) consistently mitigates the representation gap by reducing the pair-wise distance over diverse types of perturbations.

B.3. Full Results with LLaVA-v1.5-7B and LLaVA-v1.5-13B

Table 11 summarizes the overall results of our perturbation benchmarks on object hallucination detection (POPE) and open-ended QA tasks (LB-COCO). We note two findings here: (1) weight-space regularization methods, such as LoRA and WD failed to achieve reasonable performance; (2) although information maximization-based instruction tuning methods, such as ROSS and LIT, somewhat improve performance on POPE and its perturbation datasets, they greatly underperform `Vittle`, indicating a non-trivial challenge to design a versatile instruction tuning objective that can improve MLLMs on broad tasks. Meanwhile, we explore whether `Vittle` can be effective for a much larger model, e.g., a 13B-scale model. Table 12 shows that `Vittle` achieves consistent performance gains in object hallucination detection and open-ended QA tasks under distribution shifts, implying the scalability of our method.

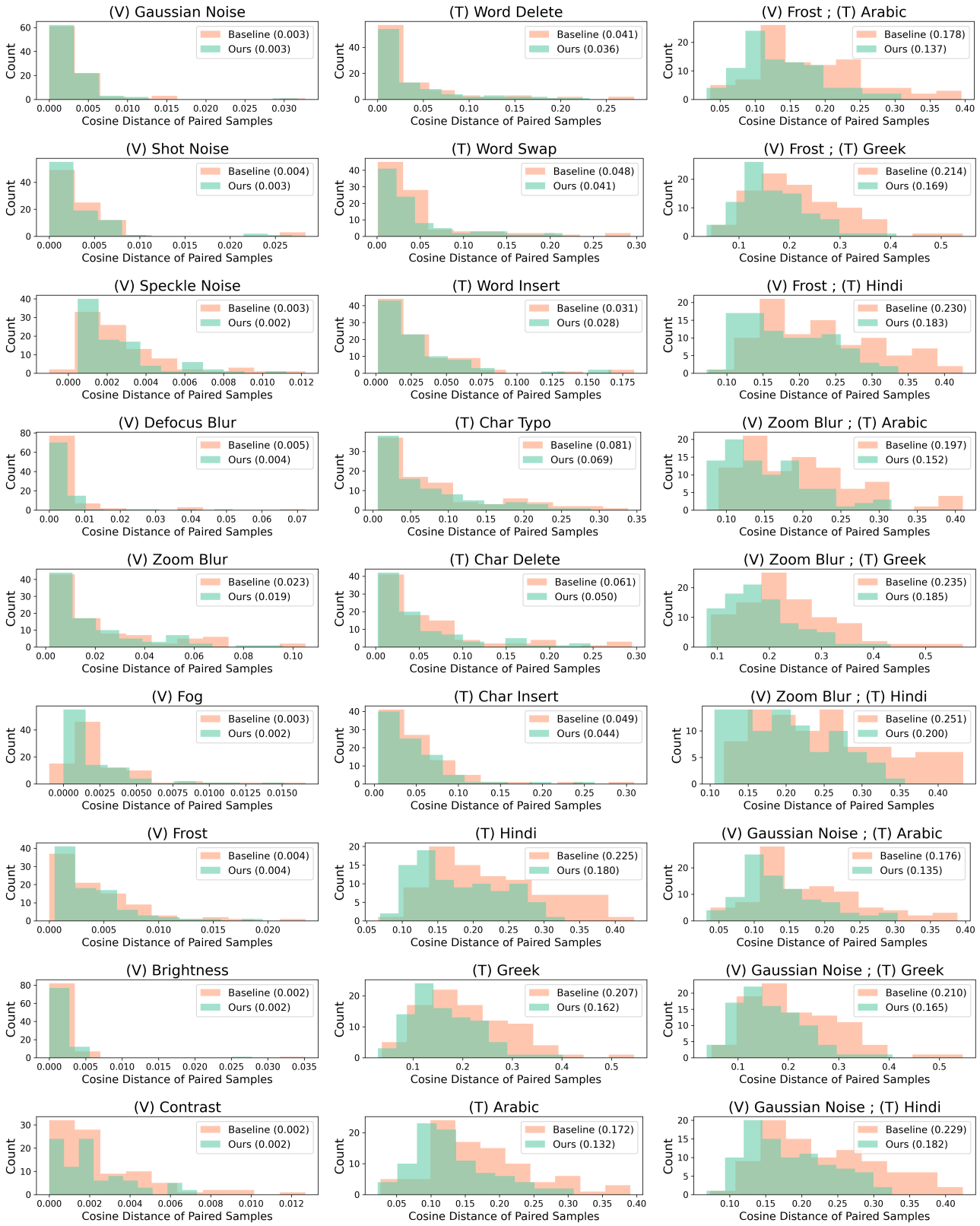

Figure 13: **Pair-wise cosine distance of intermediate representations between clean LB-COCO and 27 versions of perturbed LB-COCO datasets.** `Vittle` (F) consistently reduces the representation gap between the clean samples and their semantically equivalent perturbed ones.

B.4. Applicability to Other MLLMs

We now investigate Vittle's effectiveness on another recent MLLM, Prism-7B, beyond LLaVA. As noted in Section A.1, Prism has quite a different design principle than LLaVA with respect to the visual encoder and the training strategy, so it is suitable for investigating the versatility of Vittle between models. Table 13 shows summarized results on our perturbation benchmarks[11]. In object hallucination detection tasks, Vittle outperforms the standard cross-entropy only training baseline on clean and perturbed datasets. In open-ended QA tasks, Vittle consistently boosts performance in perturbation scenarios with large margins while maintaining performance on the clean dataset. The results of the perturbation-specific performance comparison are provided in Figure 14.

Table 13: **Vittle on Prism-7B model.** We compare Vittle (F) with the standard learning objective under the Prism-7B model training regime that adopts two visual encoders (DINOv2 and SigLIP) and the single-stage training rather than two-stage training with a single CLIP visual encoder. Vittle significantly improves perturbation-robustness compared with a naive learning objective.

Method	POPE	POPE V Pert.	LB-COCO	LB-COCO V Pert.	LB-COCO T Pert.	LB-COCO J Pert.
Baseline	87.54	85.29	79.4	75.3	71.9	53.8
Vittle (F)	88.11	85.52	79.0	76.2	75.4	63.2

[11]Due to resource constraints, we only explore Vittle (F) one of our prior distribution instantiations.

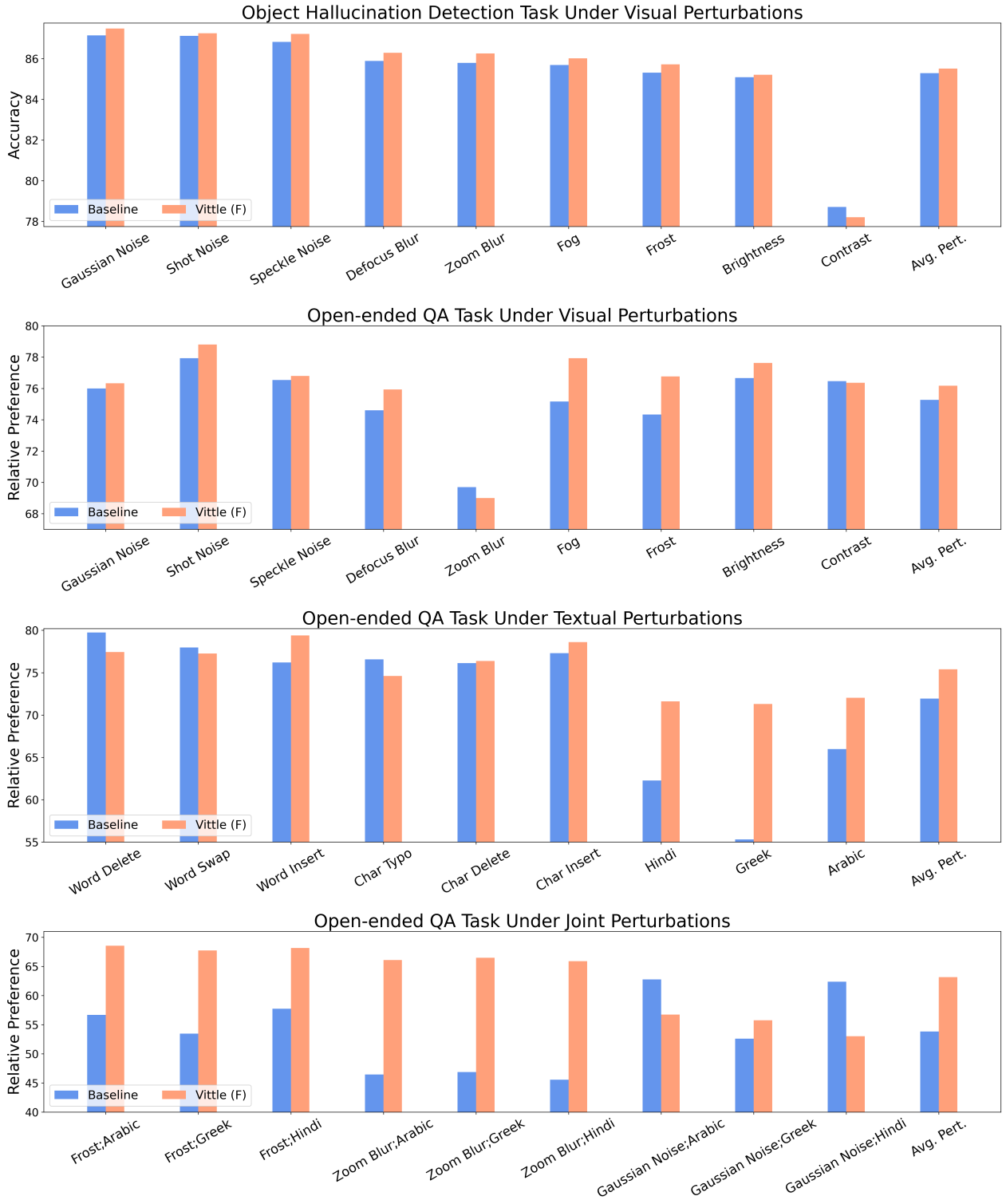

Figure 14: **Object hallucination detection performance on POPE perturbation datasets (top), and Open-ended QA performance on LB-COCO perturbation datasets (three below) of Prism-7B**. We enumerate the accuracy for the object hallucination detection task and relative preference score for the open-ended QA task of each method on perturbed datasets, where we observe consistent performance gains by `Vittle`.

C. Derivation of Variational Bound for IB in MLLM

Here we provide a full derivation for the variational lower bound for IB. The derivation skeleton was mainly inspired by existing works (Achille & Soatto, 2018; Alemi et al., 2017). We begin with the mutual information term $I(Z, X)$. Given the sequential nature of MLLM, we decompose both the input $X = (X_v, X_t)$ and the latent representation $Z = (Z_v, Z_t)$ into **v**isual and **t**extual components. We can then derive the following upper bound for $I(Z, X)$:

$$
\begin{aligned}
I(Z,X) &= \int p(x,z)\log\frac{p(x,z)}{p(x)p(z)}dxdz = \int p(x,z)\log\frac{p(z|x)}{p(z)}dxdz \\
&= \int p(x,z)\log\frac{p(z|x)}{r(z)}dxdz - D_{\mathrm{KL}}(p(z)||r(z)) \\
&\leq \int p(x,z)\log\frac{p(z|x)}{r(z)}dxdz \\
&= \int p(x_v,x_t,z_v,z_t)\log\frac{p(z_t|x_v,x_t)p(z_v|x_v)}{r(z_v)r(z_t)}dx_v dx_t dz_v dz_t \\
&= \int p(x_v,x_t)\int p(z_t|x_v,x_t)\int p(z_v|x_v)\log\frac{p(z_v|x_v)}{r(z_v)}dx_v dx_t dz_v dz_t \\
&+ \int p(x_v,x_t)\int p(z_v|x_v)\int p(z_t|x_v,x_t)\log\frac{p(z_t|x_v,x_t)}{r(z_t)}dx_v dx_t dz_v dz_t \\
&= \mathbb{E}_{x_v}[D_{\mathrm{KL}}(p(z_v|x_v)||r(z_v))] + \mathbb{E}_{x_v,x_t}[D_{\mathrm{KL}}(p(z_t|x_v,x_t)||r(z_t))],
\end{aligned} \tag{9}
$$

where the first inequality holds given the non-negativity of $D_{\mathrm{KL}}[r(z), p(z)]$ and $p(z_v|x_v, x_t) = p(z_v|x_v)$ due to causal attention in MLLM. Here, we introduce $r(z) = r(z_v, z_t) = r(z_v)r(z_t)$ as a factorizable variational approximation of the true prior for the latent representation $p(z)$.

Next, for the output-relevant term $I(Z, Y)$, we have the lower bound:

$$
\begin{aligned}
I(Z,Y) &= \int p(y,z)\log\frac{p(y,z)}{p(y)p(z)}dydz = \int p(y,z)\log\frac{p(y|z)}{p(y)}dydz \\
&= \int p(y,z)\log q(y|z)dydz + D_{\mathrm{KL}}(p(y|z)||q(y|z)) - \int p(y)\log p(y)dy \\
&\geq \int p(y,z)\log q(y|z)dydz \\
&= \int p(x,y,z)\log q(y|z)dxdydz = \int p(x)p(y|x)p(z|x)\log q(y|z)dxdydz, \\
&= \mathbb{E}_{x,y}\mathbb{E}_{z|x}\left[\log q(y|z)\right].
\end{aligned} \tag{10}
$$

where $p(x, y, z) = p(x)p(z|x)p(y|x)$ given the Markov chain assumption $Y \leftrightarrow X \leftrightarrow Z$, and $p(z|x, y) = p(z|x)$ holds given that the representation Z can not directly depend on Y, and the entropy term of y, i.e., $\int -p(y)\log p(y)dy = H(Y)$, is ruled out due to its independence for optimization problem. Here, we replace the intractable $p(y|z)$ with a variational approximation $q(y|z)$ that will be parameterized by a model.

Finally, combining the lower bound of $I(Z, Y)$ and the upper bound of $I(Z, X)$ yields a variational lower bound for the IB objective as follows,

$$
\begin{aligned}
\mathrm{IB}(X,Y) \geq\ & \mathbb{E}_{x,y}\left[\mathbb{E}_{z|x}[\log q(y|z)]\right] \\
& - \beta\left(\mathbb{E}_{x_v}\left[D_{\mathrm{KL}}(p(z_v|x_v)||r(z_v))\right] + \mathbb{E}_{x_v,x_t}\left[D_{\mathrm{KL}}(p(z_t|x_v,x_t)||r(z_t))\right]\right).
\end{aligned} \tag{11}
$$

D. Missing Proof

D.1. Preliminary

We start by providing a definition of Mutual Information (MI) below.

Definition D.1 (**Mutual Information (MI)**)**.** For a joint distribution P_{XY} over $\mathcal{X} \times \mathcal{Y}$, the mutual information with respect to P_{XY} is defined as,

$$I(P_{XY}) := \mathbb{E}_{x,y\sim P_{XY}}[\log \frac{P_{XY}(x,y)}{P_X(x)P_Y(y)}]. \tag{12}$$

If X is an instruction and Y is a corresponding response, we regard $I(P_{XY})$ as a relevance between the instruction and the response that can be seen as a possible quantification of *instruction following* capability of MLLMs. Effective MI is defined based on the MI as follows:

Definition D.2 (**Effective Mutual Information (EMI) (Oh et al., 2025a)**)**.** Given the joint distribution P_{XY} and MLLM P_Θ parameterized with Θ, the effective mutual information between the input and model response is defined as,

$$\text{EMI}(P_{XY}; P_\Theta) := I(P_{XY_\Theta}) - I(P_{XY}), \tag{13}$$

where P_{XY_Θ} denotes the joint distribution between the input X and the output of the model Y_Θ. Although the vanilla MI can also be used as a metric to evaluate models' output response by $I(P_{XY_\Theta})$, the scale of it varies depending on the target data distribution which is undesired when our interest is to compare performance of model across multiple domains which can be addressed by EMI. Recall that we are ultimately interested in the performance difference of MLLMs across two different datasets, and this can be captured by the EMI difference (EMID) as follows:

Definition D.3 (**EMID**)**.** Let $P_\Theta : \mathcal{X} \to \mathcal{Y}$ be an MLLM with parameters Θ that produces an output response Y_Θ given an input instruction X. For joint distributions P_{XY} and Q_{XY}, effective mutual information difference of P_Θ over P and Q is defined as below,

$$\text{EMID}(P_{XY}, Q_{XY}; P_\Theta) := [I(P_{XY_\Theta}) - I(P_{XY})] - [I(Q_{XY_\Theta}) - I(Q_{XY})]. \tag{14}$$

By setting P as an instruction tuning distribution (training data) and Q as an arbitrary test time distribution (evaluation data), we prefer a model that has a smaller EMID value, which indicates better robustness under distribution shifts between P and Q. Now, based on the original theorem provided by Oh et al. (Oh et al., 2025a), we are ready to derive a new upper bound for EMID tailored to our representation-centric visual instruction tuning setup.

D.2. A New Upper Bound for Effective Mutual Information Difference

We first review Lemma 1 of Shui et al. (Shui et al., 2022) and its adapted version, a conditional entropy bound (Oh et al., 2025a) as follows,

Lemma D.4 (Lemma 1 from Shui et al. (Shui et al., 2022))**.** *Let $Z \in \mathcal{Z}$ be the real-valued integrable random variable, and denoting two distributions on a common space $\mathcal{Z}$ by P and Q such that Q is absolutely continuous w.r.t. P. If for any function f and $\lambda \in \mathbb{R}$ such that $\mathbb{E}_P[\exp(\lambda(f(z) - \mathbb{E}_P(f(z))))] < \infty$, then we have:*

$$\begin{aligned}\lambda(\mathbb{E}_{z\sim Q}[f(z)] - \mathbb{E}_{z\sim P}[f(z)]) \leq D_{\text{KL}}(Q||P) \\ + \log \mathbb{E}_{z\sim P}[\exp(\lambda(f(z) - \mathbb{E}_{z\sim P}[f(z)]))]\end{aligned}$$

Lemma D.5 (Conditional entropy bound (Oh et al., 2025a))**.** *Let $f(x) := H(Q_{Y|x})$ and $\hat{H}(Q_{Y|x}) := \max_{x\in\mathcal{X}} H(Q_{Y|x})$, given the marginal distributions P_X and Q_X, and conditional distributions $P_{Y|X}$ and $Q_{Y|X}$, according to Lemma D.4, we have a conditional upper bound:*

$$i)\ \ \mathbb{E}_{x\sim P}[H(Q_{Y|x})] - \mathbb{E}_{x\sim Q}[H(Q_{Y|x})] \leq \hat{H}(Q_{Y|\mathbf{x}})\sqrt{2D_{\text{JS}}(P_X||Q_X)}.$$

Similarly, given the marginal distribution P_X and Q_X, and an MLLM P_Θ, let $f(x) := H(P_\Theta(\cdot|x))$ and $\hat{H}(P_\Theta) := \max_{x\in\mathcal{X}} H(P_\Theta(\cdot|x))$, then, according to Lemma D.4, we have another conditional upper bound:

$$ii)\ \ \mathbb{E}_{x\sim Q}[H(P_\Theta(\cdot|x)] - \mathbb{E}_{x\sim P}[H(P_\Theta(\cdot|x))] \leq \hat{H}(P_\Theta)\sqrt{2D_{\text{JS}}(P_X||Q_X)}.$$

Next, we should also need to formulate the relationship between JSD in the input space and JSD in the representation space, which is done through Lemma D.6.

Lemma D.6. *Let $f : \mathcal{X} \to \mathcal{Z}$ be an encoder that maps an input X to a representation Z, for the input distributions P_X and Q_X and f-induced representation distribution P_Z and Q_Z, we have an inequality below,*

$$\sqrt{2D_{\text{JS}}(P_X||Q_X)} \leq \sqrt{2D_{\text{JS}}(P_Z||Q_Z)} + \sqrt{\mathbb{E}_{z\sim P}[D_{\text{KL}}(P_{X|z}||M_{X|z})] + \mathbb{E}_{z\sim Q}[D_{\text{KL}}(Q_{X|z}||M_{X|z})]} \tag{15}$$

where $M_{X|z} := \frac{P_{X|z} + Q_{X|z}}{2}$.

Proof. We start from the definition of JSD,

$$D_{\text{JS}}(P_X||Q_X) = \frac{1}{2}D_{\text{KL}}(P_X||M_X) + \frac{1}{2}D_{\text{KL}}(Q_X||M_X), \quad M_X = \frac{P_X + Q_X}{2}.$$

By applying the chain rule of KLD under a deterministic map $X \to Z = f(X)$, we know that,

$$\begin{aligned} D_{\text{KL}}(P_{XZ}||M_{XZ}) &= D_{\text{KL}}(P_Z||M_Z) + \int P_Z(z)D_{\text{KL}}(P_{X|z}||M_{X|z})dz \\ &= D_{\text{KL}}(P_X||M_X) + \cancel{\int P_X(x)D_{\text{KL}}(P_{Z|x}||M_{Z|x})dx} \\ &\Leftrightarrow D_{\text{KL}}(P_X||M_X) \end{aligned}$$

Then, we have,

$$D_{\text{JS}}(P_X||Q_X) = D_{\text{JS}}(P_Z||Q_Z) + \frac{1}{2}(\mathbb{E}_{z\sim P}[D_{\text{KL}}(P_{X|z}||M_{X|z})] + \mathbb{E}_{z\sim Q}[D_{\text{KL}}(Q_{X|z}||M_{X|z})]),$$

which results in ineq. (15) by applying the triangular inequality after multiplying 2 on both sides. □

Now we derive a new upper bound for EMID, which is defined over the representation space rather than the previous one defined over the input space (Oh et al., 2025a) in Proposition D.7.

Proposition D.7 (EMID upper bound). *Let P_Θ be an MLLM that maps $X = \{X_v, X_t\}$ to $Z = \{Z_v, Z_t\}$, and then sequentially maps Z to Y_Θ. Given joint distributions $P_{XY} = P_X \times P_{Y|X}$ and $Q_{XY} = Q_X \times Q_{Y|X}$, by assuming consistent conditional distributions over $Z_v|Z_t$, $Z_t|Z_v$, and $Y|X$ between P and Q, we have an upper bound for EMID$(P_{XY}, Q_{XY}; P_\Theta)$ as follow,*

$$\hat{H}\big(D_{\text{JS}}^{\frac{1}{2}}(P_{Z_v}||Q_{Z_v}) + D_{\text{JS}}^{\frac{1}{2}}(P_{Z_t}||Q_{Z_t}) + \sqrt{\Delta_{X|Z}}\big) + |H(P_{Y_\Theta}) - H(P_Y)| + |H(Q_{Y_\Theta}) - H(Q_Y)|, \tag{16}$$

where H and $D_{\text{JS}}^{\frac{1}{2}}$ indicate the entropy and square root of Jensen-Shannon divergence (JSD), respectively, $\Delta_{X|Z} := \mathbb{E}_{z\sim P}[D_{\text{KL}}(P_{X|z}||M_{X|z})] + \mathbb{E}_{z\sim Q}[D_{\text{KL}}(Q_{X|z}||M_{X|z})]$ with a mixture distribution $M = \frac{P+Q}{2}$, and $\hat{H} := \max_{x\in\mathcal{X}}[H(Q_{Y|x}) + H(P_{Y_\Theta})]$.

Proof. Given the entropy-based definition of the mutual information, $I(P_{XY}) := H(P_Y) - \mathbb{E}_{x\sim P}[H(P_{Y|x})]$, let $P_{Y_\Theta} = \mathbb{E}_{x\sim P}[P_\Theta(\cdot|x)]$ and $Q_{Y_\Theta} = \mathbb{E}_{x\sim Q}[P_\Theta(\cdot|x)]$, then, EMID can be expressed as follows,

$$\begin{aligned} &\text{EMID}(P_{XY}, Q_{XY}; P_\Theta) \\ &= \text{EMI}(P_{XY}; P_\Theta) - \text{EMI}(Q_{XY}; P_\Theta) \\ &= (H(P_{Y_\Theta}) - \mathbb{E}_{x\sim P}[H(P_\Theta(\cdot|x))] - H(P_Y) + H(P_{Y|X})) \\ &- (H(Q_{Y_\Theta}) - \mathbb{E}_{x\sim Q}[H(P_\Theta(\cdot|x))] - H(Q_Y) + H(Q_{Y|X})) \\ &\leq (H(P_{Y|X}) - H(Q_{Y|X})) + \big(\mathbb{E}_{x\sim Q}[H(P_\Theta(\cdot|x))] - \mathbb{E}_{x\sim P}[H(P_\Theta(\cdot|x))]\big) \\ &+ |H(P_{Y_\Theta}) - H(P_Y) + H(Q_Y) - H(Q_{Y_\Theta})| \\ &\leq \underbrace{(H(P_{Y|X}) - H(Q_{Y|X}))}_{\text{(A)}} + \underbrace{\big(\mathbb{E}_{x\sim Q}[H(P_\Theta(\cdot|x))] - \mathbb{E}_{x\sim P}[H(P_\Theta(\cdot|x))]\big)}_{\text{(B)}} \\ &+ |H(P_{Y_\Theta}) - H(P_Y)| + |H(Q_Y) - H(Q_{Y_\Theta})|. \end{aligned} \tag{17}$$

Moreover, we have the following inequality for $H(P_{Y|X})$ proposed by (Oh et al., 2025a),

$$H(P_{Y|X}) - H(Q_{Y|X}) \leq 4\mathbb{E}_{x\sim P}[D_{\text{JS}}^{\frac{1}{4}}(P_{Y|x}||Q_{Y|x})] + \mathbb{E}_{x\sim P}[H(Q_{Y|x})] + \mathbb{E}_{x\sim Q}[H(Q_{Y|x})] \tag{18}$$

By plugging inequalities in Lemma D.5 and ineq. (18) into the ineq. (17) to replace the terms (A) and (B), and given the consistent conditional distribution assumption for $Y|X$, i.e., $P_{Y|X} = Q_{Y|X}$, we have a much simpler upper bound as follows,

$$\text{EMID}(P_{XY}, Q_{XY}; P_\Theta) \leq \hat{H}\sqrt{2D_{\text{JS}}(P_X||Q_X)} + |H(P_{Y_\Theta}) - H(P_Y)| + |H(Q_Y) - H(Q_{Y_\Theta})|,$$

where $\hat{H} := \max_{x\in\mathcal{X}}[H(Q_{Y|x}) + H(P_{Y_\Theta})]$. Then, we can further replace the term $D_{\text{JS}}(P_X||Q_X)$ by using Lemma D.6 to get a bound defined by representation divergence as below,

$$\begin{aligned}
&\text{EMID}(P_{XY}, Q_{XY}; P_\Theta) \\
&\leq \hat{H}(\sqrt{2D_{\text{JS}}(P_Z||Q_Z)} + \sqrt{\mathbb{E}_{z\sim P}[D_{\text{KL}}(P_{X|z}||M_{X|z})] + \mathbb{E}_{z\sim Q}[D_{\text{KL}}(Q_{X|z}||M_{X|z})]}) \\
&+ |H(P_{Y_\Theta}) - H(P_Y)| + |H(Q_Y) - H(Q_{Y_\Theta})|.
\end{aligned} \tag{19}$$

Meanwhile, the chain rule of KLD and the definition of JSD with our consistent conditional distributions for $Z_v|Z_t$ and $Z_t|Z_v$, one can easily show that,

$$\begin{aligned}
2D_{\text{JS}}(P_{Z_vZ_t}||Q_{Z_vZ_t}) &= D_{\text{KL}}(P_{Z_vZ_t}||M_{Z_vZ_t}) + D_{\text{KL}}(Q_{Z_vZ_t}||M_{Z_vZ_t}) \\
&= D_{\text{JS}}(P_{Z_v}||Q_{Z_v}) + D_{\text{JS}}(P_{Z_t}||Q_{Z_t})
\end{aligned} \tag{20}$$

Plugging Eq. 20 into ineq. (19) and applying the triangular inequality complete the proof. □

E. Extended Literature Review

Compression for generalization. There is a rich history in the machine learning field that connects compression of the model or its inner representation to generalization (Arora et al., 2018), from the classical learning theory with *Occam's razor* (Littlestone & Warmuth, 1986; Blumer et al., 1987) and *Minimal Description Length* (Rissanen, 1978; Hinton & Van Camp, 1993; Grünwald, 2005) to *IB principle* (Tishby et al., 2000; Tishby & Zaslavsky, 2015), by suggesting models that provide minimal and simplest representation of data generalize better (Vera et al., 2018; Hinton & Van Camp, 1993; Kawaguchi et al., 2023; Sefidgaran et al., 2023) analogy to human perception (Miller, 1956; Barlow et al., 1961; Zhaoping, 2025). Recently, Wilson (Wilson, 2025) proposed a new generalization bound for contemporary large-scale models where the ***compressibility*** of a learning algorithm plays a key role in better generalization. According to that discussion, even the maximally flexible billion-scale model can have a small effective dimensionality (indicating the higher compressibility) by embracing *soft inductive biases* (Finzi et al., 2021), such as, a regularization term, to the learning problem. On top of these, IB-objective of `Vittle` can be understood as a soft inductive bias to seek a minimal sufficient representation that helps generalization for the challenging queries.

Robustness of fine-tuned foundation models. Although large-scale pre-trained models have appealing generalization capability across diverse data instances from different domains, their fine-tuned counterparts usually hurts that strong generalization capability while being adapting on task-specific in-distribution samples (Kumar et al., 2022; Wortsman et al., 2022). This undesirable performance compromise between adaptation to in-distribution samples and generalization to samples from broad domains has spurred the community to work on *robust fine-tuning* of foundation models (Kumar et al., 2022; Wortsman et al., 2022; Lee et al., 2023; Goyal et al., 2023; Tian et al., 2023; Oh et al., 2024; Hwang et al., 2024). This line of work addresses the adaptation-robustness trade-off by (1) introducing a regularization term (Tian et al., 2023; Oh et al., 2024), (2) tweaking the training procedure (Kumar et al., 2022; Lee et al., 2023), or (3) merging multiple models in the weight space (Wortsman et al., 2022; Oh et al., 2025b). However, almost all of the existing robust fine-tuning literature has focused on a discriminative model, such as CLIP (Radford et al., 2021), under classification setups. Although there are a few works on robust instruction tuning of MLLMs (Liu et al., 2024a; Han et al., 2024a), they do not specifically focus on improving robustness under diverse types of distribution shifts and propose a *data-centric approach*, i.e., expanding instruction tuning datasets in terms of quantity or diversity, that requires external MLLM-based data generation process and/or careful post-processing from humans. In this work, we take a *representation-centric* approach that modifies the learning objective of visual instruction tuning to efficiently enhance the robustness of MLLM under diverse distribution shifts (27 types in total).

F. Limitation and Future Work

One of the potential concerns with IB is its reliance on the quality of Y, i.e., a gold response to given instruction, which is usually generated by another (M)LLM. As disclosed by Yeh et al. (Yeh et al., 2025), the existing datasets for supervised fine-tuning are quite noisy, and we cannot ensure the advantage of IB on this noisy annotation setup. Moreover, IB alone does not guarantee the generalization of samples from completely different domains and may require additional domain information (Du et al., 2020; Li et al., 2022a; Zhang et al., 2023). Investigating the potential of noisy annotation setups and domain generalization setups can be interesting future research problems. Meanwhile, a well-organized representation space by IB can be helpful for representation engineering or steering methods (Zou et al., 2023; Liu et al., 2025) that are also worth exploring for future work.

G. Impact Statement

Multimodal large language models (MLLMs) today have many societal applications. This work tackles the robustness of MLLMs to distribution shifts between training and test time data. We observed a consistent improvement of our proposal `Vittle` in various types of visual and textual shifts, allowing users to trust the model more than before to safely use AI in a variety of environments. Moreover, although we focused on the robustness perspective in this work, improved invariance-sensitivity trade-off also benefits the fairness-discriminativeness trade-off, which is another crucial desideratum towards reliable AI. Meanwhile, even though its robustness to distribution shifts was improved, there are still potential misuse cases with MLLMs that can affect humanity by producing systematically biased outputs, given the existence of some adversarial data providers or attackers.